

# **An Effective Model of the Retinoic Acid Induced HL-60 Differentiation Program**

Ryan Tasseff, Holly A. Jensen, Johanna Congleton<sup>†</sup>, Wei Dai, Katherine Rogers, Adithya Sagar, Rodica P. Bunaciu<sup>†</sup>, Andrew Yen<sup>†</sup>, and Jeffrey D. Varner\*

Robert Frederick Smith School of Chemical and Biomolecular Engineering and <sup>†</sup>Department of Biomedical Sciences, Cornell University, Ithaca NY 14853

**Running Title:** Effective modeling of HL-60 differentiation

**To be submitted:** ?

\*Corresponding author:

Jeffrey D. Varner,

Professor, Robert Frederick Smith School of Chemical and Biomolecular Engineering,  
244 Olin Hall, Cornell University, Ithaca NY, 14853

Email: jdv27@cornell.edu

Phone: (607) 255 - 4258

Fax: (607) 255 - 9166

## Abstract

In this study, we present an effective model All-Trans Retinoic Acid (ATRA)-induced differentiation of HL-60 cells. The model describes a key architectural feature of ATRA-induced differentiation, reinforcing feedback between an ATRA-inducible signalsome complex involving many proteins including Vav1, a guanine nucleotide exchange factor, and the activation of the mitogen activated protein kinase (MAPK) cascade. We decomposed the effective model into three modules; a signal initiation module that sensed and transformed an ATRA signal into program activation signals; a signal integration module that controlled the expression of upstream transcription factors; and a phenotype module which encoded the expression of functional differentiation markers from the ATRA-inducible transcription factors. The model, which was developed by integrating logical rules with kinetic modeling, was significantly smaller than previous models. However, despite its simplicity, it captured key features of ATRA induced differentiation of HL-60 cells. We identified an ensemble of effective model parameters using measurements taken from ATRA-induced HL-60 cells. Using these parameters, model analysis predicted that MAPK activation was bistable as a function of ATRA exposure. Conformational experiments supported ATRA-induced bistability. Additionally, the model captured intermediate and phenotypic gene expression data. Knockout analysis of the model suggested Gfi-1 and PPAR $\gamma$  were critical to the ATRA-induced differentiation program. These findings, combined with other literature evidence, suggested that reinforcing feedback is central to a diversity of cell fate programs.

## **1 Introduction**

2 Understanding the architecture of differentiation programs is an important therapeutic  
3 challenge. Differentiation induction chemotherapy (DIC), using agents such as the vi-  
4 tamin A derivative all-trans retinoic acid (ATRA), is a promising approach for the treat-  
5 ment of many cancers (1–3). For example, ATRA treatment induces remission in 80–90%  
6 of promyelocytic leukemia (APL) PML-RAR $\alpha$ -positive patients (4), thereby transforming  
7 a fatal diagnosis into a manageable disease (5). However, remission is sometimes not  
8 durable and relapsed cases exhibit emergent ATRA resistance (6, 7). To understand  
9 the basis of this resistance, we must first understand the ATRA-induced differentiation  
10 program. Toward this challenge, lessons learned in model systems, such as the lineage-  
11 uncommitted human myeloblastic cell line HL-60 reported to closely resemble patient  
12 derived cells (8), could inform our analysis of the differentiation programs occurring in  
13 patients. Patient derived HL-60 leukemia cells have been a durable experimental model  
14 since the 1970's to study differentiation (9). HL-60 undergoes cell cycle arrest and either  
15 myeloid or monocytic differentiation following stimulation; ATRA induces G1/G0-arrest and  
16 myeloid differentiation in HL-60 cells, while 1,25-dihydroxy vitamin D3 (D3) induces arrest  
17 and monocytic differentiation. Commitment to cell cycle arrest and differentiation requires  
18 approximately 48 hr of treatment, during which HL-60 cells undergo two division cycles.

19 Sustained mitogen-activated protein kinase (MAPK) activation is a defining feature of  
20 ATRA-induced HL-60 differentiation. ATRA drives sustained activation of the Raf/MEK/ERK  
21 pathway, leading to arrest and differentiation (10). Betraying a feedback loop, MEK inhi-  
22 bition results in the loss of ERK and Raf phosphorylation, and the failure to arrest and  
23 differentiate in response to ATRA (11). Retinoic acid (and its metabolites) are ligands  
24 for the hormone activated nuclear transcription factors retinoic acid receptor (RAR) and  
25 retinoid X receptor (RXR) (12). RAR/RXR activation is necessary for ATRA-induced Raf  
26 phosphorylation (11), and the formation of an ATRA-inducible signalsome complex at the

membrane, which drives MAPK activation. While the makeup of the signalsome complex is not yet known, we do know that it is composed of Src family kinases Fgr and Lyn, PI3K, c-Cbl, Slp76, and KSR, plus transcription factors AhR and IRF1 (13–17). Signalsome activity is driven by ATRA-induced expression of CD38 and putatively the heterotrimeric Gq protein-coupled receptor BLR1 (18, 19). BLR1 (also known as CXCR5), identified as an early ATRA (or D3)-inducible gene using differential display (20), is necessary for MAPK activation and differentiation (19), and drives signalsome activity. Studies of the BLR1 promoter identified a non-canonical RARE site consisting of a 17 bp GT box approximately 1 kb upstream of the transcriptional start that conferred ATRA responsiveness (19). Members of the BLR1 transcriptional activator complex, e.g. NFATc3 and CREB, are phosphorylated by ERK, JNK or p38 MAPK family members suggesting positive feedback between the signalsome and MAPK activation (21). BLR1 overexpression enhanced Raf phosphorylation and accelerated terminal differentiation, while Raf inhibition reduced BLR1 expression and ATRA-induced terminal differentiation (22). In particular, Raf phosphorylation of the NFATc3 transcription factors at the BLR1 promoter enables transcriptional activation at the RARE by ATRA bound to RAR/RXR (23). BLR1 knock-out cells failed to activate Raf or differentiate in the presence of ATRA (22). Interestingly, both the knockdown or inhibition of Raf, also reduced BLR1 expression and functional differentiation (22). Thus, the expression of signalsome components e.g., BLR1 was Raf dependent, while Raf activation depended upon the signalsome. A previous computational study of ATRA-induced differentiation of HL-60 cells suggested that the BLR1-MAPK positive feedback circuit was sufficient to explain ATRA-induced sustained MAPK activation, and the expression of a limited number of functional differentiation markers (24). Model analysis also suggested that Raf was the most distinct of the MAPK proteins. However, this previous study developed and analyzed a complex model, thus leaving open the critical question of what is the minimal positive feedback circuit required to drive ATRA-induced

53 differentiation.

54 In this study, we explored this question using a minimal mathematical model of the  
55 key architectural feature of ATRA induced differentiation of HL-60 cells, namely positive  
56 feedback between an ATRA-inducible signalsome complex and MAPK activation. The  
57 ATRA responsive signalsome-MAPK circuit was then used to drive a downstream gene  
58 expression program which encoded for the expression of intermediate and functional dif-  
59 ferentiation markers. The effective model used a novel framework which integrated logi-  
60 cal rules with kinetic modeling to describe gene expression and protein regulation, while  
61 largely relying upon biophysical parameters from the literature. This formulation signif-  
62 icantly reduced the size and complexity of the model compared to the previous study  
63 of Tasseff et al., while increasing the breadth of the biology described (24). The effec-  
64 tive model, despite its simplicity, captured key features of ATRA induced differentiation of  
65 HL-60 cells. Model analysis predicted the bistability of MAPK activation as a function of  
66 ATRA exposure; conformational experiments supported ATRA-induced bistability. Model  
67 simulations were also consistent with measurements of the influence of MAPK inhibitors,  
68 and the failure of BLR1 knockout cells to differentiate when exposed to ATRA. In addition,  
69 the expression of intermediate and phenotypic differentiation markers as also captured  
70 following ATRA exposure. Lastly, we showed through immunoprecipitation and inhibitor  
71 studies, that the guanine nucleotide exchange factor Vav1 is potentially a new ATRA-  
72 inducible member of the signalsome complex functioning as a regulator that contributes  
73 to signal amplification in the signalsome. Taken together, these findings when combined  
74 with other literature evidence, suggested that positive feedback architectures are central  
75 to differentiation programs generally, and necessary for ATRA-induced differentiation. The  
76 model answers a biologically important question that is not easily experimentally attacked,  
77 namely given the complexity of the signaling machine and the pathways it embodies, is  
78 there a critical small suite of molecules that are the action elements seminal to eliciting

<sup>79</sup> ATRA-induced cell differentiation and G0 arrest.

80 **Results**

81 We constructed an effective model of ATRA-induced HL-60 differentiation which described  
82 signaling and gene expression events following the addition of ATRA (Fig. 1). The model  
83 connectivity was developed from literature and the studies presented here (Table 1). We  
84 decomposed the ATRA program into three modules; a signal initiation module that sensed  
85 and transformed the ATRA signal into activated cRaf-pS621 and the ATRA-RAR/RXR  
86 (Trigger) signals (Fig. 1A); a signal integration module that controlled the expression  
87 of upstream transcription factors given cRaf-pS621 and activated Trigger signals (Fig.  
88 1B); and a phenotype module which encoded the expression of functional differentiation  
89 markers from the ATRA-inducible transcription factors (Fig. 1C). In particular, Trigger (a  
90 surrogate for the RAR $\alpha$ /RXR transcriptional complex) regulated the expression of the tran-  
91 scription factors CCATT/enhancer binding protein  $\alpha$  (C/EBP $\alpha$ ), PU.1, and Egr-1. In turn,  
92 these transcription factors, in combination with cRaf-pS621, regulated the expression of  
93 downstream phenotypic markers such as CD38, CD11b or p47Phox. Each component of  
94 these modules was described by a mRNA and protein balance equation. Additionally, the  
95 signal initiation module also described the abundance of activated species e.g., Trigger  
96 and cRaf-pS621 whose values were derived from unactivated Trigger and cRaf protein  
97 levels. Lastly, because the population of HL-60 cells was dividing, we also considered  
98 a dilution term in all balance equations. The signal initiation module contained nine dif-  
99 fferential equations, while the signal integration and phenotype modules were collectively  
100 encoded by 54 differential equations. Model parameters were taken from literature (Table  
101 2), or estimated from experimental data using heuristic optimization (see materials and  
102 methods).

103 The signal initiation module recapitulated sustained signalsome and MAPK activation  
104 following exposure to 1 $\mu$ M ATRA (Fig. 2A-B). An ensemble of effective model param-  
105 eters was estimated by minimizing the difference between simulations and time-series

106 measurements of BLR1 mRNA and cRaf-pS621 following the addition of  $1\mu\text{M}$  ATRA. We  
107 focused on the S621 phosphorylation site of cRaf since enhanced phosphorylation at this  
108 site is a defining characteristic of sustained MAPK signaling activation in HL-60. The  
109 effective model captured both ATRA-induced BLR1 expression (Fig. 2A) and sustained  
110 phosphorylation of cRaf-pS621 (Fig. 2B) in a growing population of HL-60 cells. To-  
111 gether, the reinforcing feedback within the signalsome and its embedded MAPK signaling  
112 axis led to sustained activation over multiple cellular generations. However, the effective  
113 model failed to capture the decline of BLR1 message after 48 hr of ATRA exposure. This  
114 suggested that we captured the logic leading to the onset of differentiation, but failed to  
115 describe program shutdown. Much of the focus in the literature has been on understand-  
116 ing the initiation of differentiation, with little attention paid to understanding how a program  
117 is terminated. This is a potential new direction that could be explored. Next, we tested  
118 the response of the signal initiation module to different ATRA dosages.

119 The signal initiation model was bistable with respect to ATRA induction (Fig. 2C-D).  
120 Phaseplane analysis predicted two stable steady-states when ATRA was present below  
121 a critical threshold (Fig. 2C), and only a single steady-state above the threshold (Fig.  
122 2D). In the lower stable state, neither the signalsome nor cRaf-pS621 were present (thus,  
123 the differentiation program was inactive). However, at the higher stable state, both the  
124 signalsome and cRaf-pS621 were present, allowing for sustained activation and differen-  
125 tiation. Interestingly, when ATRA was above a critical threshold, only the activated state  
126 was accessible (Fig. 2D). To test these findings, we first identified the ATRA threshold. We  
127 exposed HL-60 cells to different ATRA concentrations for 72 hr (Fig. 2E). Morphological  
128 changes associated with differentiation were visible for  $\text{ATRA} \geq 0.25\mu\text{M}$ , suggesting the  
129 critical ATRA threshold was near this concentration. Next, we conducted ATRA washout  
130 experiments to determine if activated cells remained activated in the absence of ATRA.  
131 HL-60 cells locked into an activated state remained activated following ATRA withdraw

132 (Fig. 3C). This sustained activation resulted from reinforcing feedback between the sig-  
133 nalsome and the MAPK pathway. Thus, following activation, if we inhibited or removed  
134 elements from the signal initiation module we expected the signalsome and MAPK signals  
135 to decay. We simulated ATRA induced activation in the presence of kinase inhibitors, and  
136 without key circuit elements. Consistent with experimental results using multiple MAPK  
137 inhibitors, ATRA activation in the presence of MAPK inhibitors lowered the steady-state  
138 value of signalsome (Fig. 3A). In the presence of BLR1, the signalsome and cRaf-pS621  
139 signals were maintained following ATRA withdraw (Fig. 3B, gray). On the other hand,  
140 BLR1 deletion removed the ability of the circuit to maintain a sustained MAPK response  
141 following the withdraw of ATRA (Fig. 3B, blue). Lastly, washout experiments in which  
142 cells were exposed to  $1\mu\text{M}$  ATRA for 24 hr, and then transferred to fresh media with-  
143 out ATRA, confirmed the persistence of the self sustaining activated state for up to 144  
144 hr (Fig. 3C). Thus, these experiments confirmed that reinforcing positive feedback likely  
145 drives the ATRA-induced differentiation program. Next, we analyzed the ATRA-induced  
146 downstream gene expression program following signalsome and cRaf activation.

147 The signal integration and phenotype modules described ATRA-induced gene expres-  
148 sion in wild-type HL-60 cells (Fig. 4). The signal initiation module produced two outputs,  
149 activated Trigger and cRaf-pS621 which drove the expression of ATRA-induced transcrip-  
150 tion factors, which then in turn activated the phenotypic program. We assembled the  
151 connectivity of the signal integration and phenotypic programs driven by Trigger and cRaf-  
152 pS621 from literature (Table 1). We estimated the parameters for the signal initiation, and  
153 phenotype modules from steady-state and dynamic measurements of transcription factor  
154 and phenotypic marker expression following the addition of ATRA (25–28). However, the  
155 bulk of the model parameters were taken from literature (29) and were not estimated in  
156 this study (see materials and methods). The model simulations captured the time de-  
157 pendent expression of CD38 and CD11b following the addition ATRA (Fig. 4A), and the

158 steady-state for signal integration and phenotypic markers (Fig. 4B). Lastly, we used the  
159 *predicted* values of the p21 and E2F protein abundance to estimate a blackbox model of  
160 ATRA-induced G0 arrest (Fig. 5). The phenotype module predicted p21 expression sig-  
161 nificantly increased and E2F expression decreased, in response to ATRA exposure (Fig.  
162 5A). We then used the ratio of these values in a polynomial model to calculate the frac-  
163 tion of HL-60 cells in G0 arrest following the addition of ATRA (Fig. 5B). The third-order  
164 polynomial model captured the trend in measured G0-arrest values as a function of time,  
165 and was robust to uncertainty in the measured data (Fig. 5B, gray). Taken together, the  
166 output of the signal integration and phenotypic modules was consistent with time-series  
167 and steady-state measurements, thereby validating the assumed molecular connectivity.  
168 Moreover, outputs from the phenotype module described the trend in ATRA-induced G0  
169 cell cycle arrest. Next, we explored which proteins and protein interactions in the signal  
170 integration module most influenced the system response.

171 The Gfi-1 and PPAR $\gamma$  proteins were important regulators of ATRA-induced signal in-  
172 tegration and phenotypic change (Fig. 6). We conducted pairwise gene knockout simu-  
173 lations in the signal integration and phenotype modules to estimate which proteins con-  
174 trolled the processing of the Trigger and cRaf-S621 signals. The difference between the  
175 system state with and without the gene knockouts (encoded as a normalized state dis-  
176 placement matrix) was decomposed using Singular Value Decomposition (SVD). A panel  
177 of ten parameter sets was sampled, and the average normalized displacement matrix  
178 was decomposed. The first six modes (approximately 36% of the total) described >95%  
179 of the gene knockout variance, with the most important components of these modes be-  
180 ing the Gfi-1 and PPAR $\gamma$  proteins, and to a lesser extent PU.1, C/EBP $\alpha$  and AP1  
181 (Fig. 6A). To better understand which protein-DNA connections were important, we sim-  
182 ulated the pairwise deletion of interactions between these proteins and their respective  
183 regulatory targets. Singular value decomposition of the normalized state displacement

matrix assembled from the pairwise connection deletions, suggested the first six modes (approximately 26% of the total) accounted for >90% of the variance. Globally, the most sensitive interactions controlled p21 and p47Phox expression, markers for cell-cycle arrest and reactive oxygen formation phenotypic axes activated following ATRA addition (Fig. 6B). Analysis of the modes suggested the action of PPAR $\gamma$ , Gfi-1 and C/EBP $\alpha$  were consistently important over multiple target genes. The connection knockout analysis also revealed robustness in the network. For example, no pair of deletions qualitatively changed the expression of regulators such as PU.1, Oct1, Oct4 or PPAR $\gamma$ . Thus, the expression of these species was robust to disturbance in the connectivity. To better understand the combined influence of the PPAR $\gamma$  and Gfi-1 deletions, we computed the fold change in the protein levels in the single (Gfi-1 $^{-/-}$  or PPAR $\gamma$  $^{-/-}$ ) and double (Gfi-1 $^{-/-}$  and PPAR $\gamma$  $^{-/-}$ ) mutants for the best fit parameter set (Fig. 7). Deletion of Gfi-1 led to a 2-4 fold increase in EGR-1, CD11b and C/EBP $\alpha$  expression, and a >8 fold increase in PU.1 abundance (Fig. 7,blue). On the other hand, deletion of PPAR $\gamma$  led to >8 fold down-regulation of CD38, p21, IRF1 and Oct1 (Fig. 7,red). Both knockouts slightly increased E2F expression, but neither influenced the expression of p47Phox. The double mutant was qualitatively similar to the combined behavior of the two single mutant cases. Taken together, Gfi-1 and PPAR $\gamma$  controlled the cell-cycle arrest and receptor signaling axes, with PPAR $\gamma$  regulating CD38, IRF1 and p21 expression while Gfi-1 controlled CD11b expression. These simulations suggested deletion of PPAR $\gamma$  and Gfi-1 would not interfere with reactive oxygen formation, but would limit the ability of HL-60 cells to arrest. However, this analysis did not give insight into which components upstream of the signal initiation module were important. Toward this question, we explored the composition and regulation of the signalsome complex by experimentally interrogating a panel of possible Raf interaction partners.

The full composition of the signalsome, and the kinase therein ultimately responsible

for mediating ATRA-induced Raf activation is currently unknown. To explore this question, we conducted immunoprecipitation and subsequent Western blotting to identify physical interactions between Raf and 19 putative interaction partners. A panel of 19 possible Raf interaction partners (kinases, GTPases, scaffolding proteins etc) was constructed based upon known signaling pathways. We did not consider the most likely binding partner, the small GTPase RAS, as previous studies have ruled it out in MAPK activation in HL-60 cells (22, 30). Total Raf was used as a bait protein for the immunoprecipitation studies. Interrogation of the Raf interactome suggested Vav1 was involved with ATRA-induced initiation of MAPK activity (Fig. 8). Western blot analysis using total Raf and Raf-pS621 specific antibodies confirmed the presence of the bait protein, total and phosphorylated forms, in the immunoprecipitate (Fig. 8A). Of the 19 proteins sampled, Vav1, Src, CK2, Akt, and 14-3-3 co-precipitated with Raf, suggesting their co-existence in a complex was possible. However, only the associations between Raf and Vav1, and Raf and Src were ATRA-inducible (Fig. 8). Furthermore, the Vav1 and Src associations were correlated with Raf-pS621 abundance in the precipitate. Other proteins e.g., CK2, Akt and 14-3-3, generally bound Raf regardless of phosphorylation status or ATRA treatment. The remaining 14 proteins were expressed in whole cell lysate (Fig. 8B), but were not detectable in the immuno-precipitate with Raf IP; consistent with the potential importance of the Raf-Vav interaction for signaling, it paralleled Raf phosphorylation at S621, a putative telltale of the activated kinase. Treatment with the Raf kinase inhibitor GW5074 following ATRA exposure reduced the association of both Vav1 with Raf and Src with Raf (Fig. 8), although the signal intensity for Src was notably weak. However, GW5074 did not influence the association of CK2 or 14-3-3 with Raf, further demonstrating their independence from Raf phosphorylation. Interestingly, the Raf-Akt interaction qualitatively increased following treatment with GW5074; however, it remained unaffected by treatment with ATRA. Src family kinases are known to be important in myeloid differentiation (31) and their role

236 in HL-60 differentiation has been investigated elsewhere (13). Given the existing work  
237 and variable reproducibility in the context of the Raf immunoprecipitate, we did not investi-  
238 giate the role of Src further in this study. Taken together, the immunoprecipitation and  
239 GW5074 results implicated Vav1 association to be correlated with Raf activation following  
240 ATRA-treatment. Previous studies demonstrated that a Vav1-Slp76-Cbl-CD38 complex  
241 plays an important role in ATRA-induced MAPK activation and differentiation of HL-60  
242 cells (15). Here we did not observe direct interaction of Raf with Cbl or Slp76; however,  
243 this interaction could be involved upstream. Next, we considered the effect of the  
244 Raf kinase inhibitor GW5074 on functional markers of ATRA-induced growth arrest and  
245 differentiation.

246 Inhibition of Raf kinase activity modulated MAPK activation and differentiation mark-  
247 ers following ATRA exposure (Fig. 8D-F). ATRA treatment alone statistically significantly  
248 increased the G1/G0 percentage over the untreated control, while GW5074 alone had a  
249 negligible effect on the cell cycle distribution (Fig. 8D). Surprisingly, the combination of  
250 GW5074 and ATRA statistically significantly increased the G1/G0 population ( $82 \pm 1\%$ )  
251 compared with ATRA alone ( $61 \pm 0.5\%$ ). Increased G1/G0 arrest following the combined  
252 treatment with GW5074 and ATRA was unexpected, as the combination of ATRA and the  
253 MEK inhibitor (PD98059) has been shown previously to decrease ATRA-induced growth  
254 arrest (10). However, growth arrest is not the sole indication of functional differentiation.  
255 Expression of the cell surface marker CD11b has also been shown to coincide with HL-60  
256 cells myeloid differentiation (32). We measured CD11b expression, for the various treat-  
257 ment groups, using immuno-fluorescence flow cytometry 48 hr post-treatment. As with  
258 G1/G0 arrest, ATRA alone increased CD11b expression over the untreated control, while  
259 GW5074 further enhanced ATRA-induced CD11b expression (Fig. 8E). GW5074 alone  
260 had no statistically significant effect on CD11b expression, compared with the untreated  
261 control. Lastly, the inducible reactive oxygen species (ROS) response was used as a func-

<sup>262</sup> tional marker of differentiated neutrophils (18). We measured the ROS response induced  
<sup>263</sup> by the phorbol ester 12-O-tetradecanoylphorbol-13-acetate (TPA) using flow cytometry.  
<sup>264</sup> Untreated cells showed no discernible TPA response, with only  $7.0 \pm 3.0\%$  ROS induction  
<sup>265</sup> (Fig. 8F). Cells treated with ATRA had a significantly increased TPA response,  $53 \pm 7\%$   
<sup>266</sup> ROS induction 48 hr post-treatment. Treatment with both ATRA and GW5074 statistically  
<sup>267</sup> significantly reduced ROS induction ( $22 \pm 0.6\%$ ) compared to ATRA alone. Interestingly,  
<sup>268</sup> Western blot analysis did not detect a GW5074 effect on ATRA-induced expression of  
<sup>269</sup> p47Phox, a required upstream component of the ROS response (Fig. 8F, bottom). Thus,  
<sup>270</sup> the inhibitory effect of GW5074 on inducible ROS might occur downstream of p47Phox  
<sup>271</sup> expression. However, the ROS producing complex is MAPK dependent, therefore it is  
<sup>272</sup> also possible that GW5074 inhibited ROS production by interfering with MAPK activation  
<sup>273</sup> (in which case the p47Phox marker might not accurately reflect phenotypic conversion  
<sup>274</sup> and differentiation).

275 **Discussion**

276 In this study, we presented an effective model of ATRA-inducible differentiation of HL-60  
277 cells. The model consisted of three modules: a signal initiation module that sensed and  
278 transformed the ATRA signal into activated cRaf-pS621 and the ATRA-RAR/RXR (Trig-  
279 ger) signals; a signal integration module that controlled the expression of upstream tran-  
280 scription factors given cRaf-pS621 and activated Trigger signals; and a phenotype mod-  
281 ule which encoded the expression of functional differentiation markers from the ATRA-  
282 inducible transcription factors. The model described the transcription and translation of  
283 genes in each module, and signaling events in each module in a growing population of  
284 HL-60 cells. Model parameters were taken from literature, however, unknown coefficients  
285 that appear in the promoter logic models were estimated from protein measurements  
286 in HL-60 cells following ATRA exposure. Despite its simplicity, the effective model cap-  
287 tured key features of the ATRA induced differentiation such as sustained MAPK activation,  
288 and bistability with respect to ATRA exposure. The model also described the expression  
289 of upstream transcription factors which regulated the expression of differentiation mark-  
290 ers. Lastly, analysis of the response of the model to perturbations identified Gfi-1 and  
291 PPAR $\gamma$  as master regulators of ATRA-induced differentiation. We also found evidence  
292 of a prominent regulatory role for a signaling molecule ATRA-inducible component of the  
293 signalsome, Vav1. Vav1 is a guanine nucleotide exchange factor for Rho family GTPases  
294 that activate pathways leading to actin cytoskeletal rearrangements and transcriptional al-  
295 terations (33). The Vav1/Raf association correlated with Raf activity, was ATRA-inducible  
296 and decreased after treatment with the Raf inhibitor GW5074.

297 Naturally occurring cell fate decisions often incorporate reinforcing feedback and bista-  
298 bility (34, 35). One of the most well studied cell fate circuits is the Mos mitogen-activated  
299 protein kinase cascade in *Xenopus* oocytes. This cascade is activated when oocytes are  
300 induced by the steroid hormone progesterone (36). The MEK-dependent activation of p42

301 MAPK stimulates the accumulation of the Mos oncoprotein, which in turn activates MEK,  
302 thereby closing the feedback loop. This is similar to the signal initiation module presented  
303 here; ATRA drives signalsome formation, which activates MAPK, which in turn leads to  
304 more signalsome activation. Thus, while HL-60 and *Xenopus* oocytes are vastly different  
305 biological models, their cell fate programs share a similar architectural feature. Reinforc-  
306 ing feedback and bistability has also been implicated in hematopoietic cell fate determi-  
307 nation. Laslo et al showed in nonmalignant myelomonocytic cells that the counter antag-  
308 onistic repressors, Gfi-1 and Egr-1/2 (whose expression is tuned by PU.1 and C/EBP $\alpha$ ),  
309 encode a bistable switch that results in a macrophage, neutrophil or a mixed lineage pop-  
310 ulation depending upon PU.1 and C/EBP $\alpha$  expression (35). The current model contained  
311 the Gfi-1 and Egr-1/2 agonistic switch; however, its significance was unclear for HL-60  
312 cells. The expression of Gfi-1, Egr-1/2, C/EBP $\alpha$  and PU.1 was not consistent with the  
313 canonical lineage pattern expected from literature. For example, Egr-1/2 expression (as-  
314 sociated with a macrophage lineage) increased, while Gfi-1 expression (associated with  
315 a neutrophil lineage) was unchanged following ATRA exposure. Thus, HL-60 cells, which  
316 are a less mature cancer cell line, exhibited a non-canonical expression pattern. Other  
317 unrelated cell fate decisions such as programmed cell death have also been suggested to  
318 be bistable (37). Still more biochemical networks important to human health, for example  
319 the human coagulation or complement cascades, also feature strong positive feedback el-  
320 ements (38). Thus, while reinforcing feedback is often undesirable in human engineered  
321 systems, it is at the core of a diverse variety of cell fate programs and other networks  
322 important to human health.

323 Analysis of the signal integration and phenotype modules suggested Gfi-1 and PPAR $\gamma$   
324 proteins were important regulators of ATRA-induced signal integration and phenotypic  
325 change. Model analysis showed that PU.1, Egr-1 and C/EBP $\alpha$  expression increased in  
326 Gfi-1 $^{-/-}$  mutants, where PU.1 expression was upregulated by greater than 8-fold. PU.1, a

member of the *ets* transcription factor family, is a well known regulator of granulocyte and monocyte development (39). The relative level of PU.1 and C/EBP $\alpha$  is thought to control macrophage versus neutrophil cell fate decisions in granulocytic macrophage progenitor cells (40). Simulations suggested that combined Gfi-1 + PPAR $\gamma$  deletion crippled the ability of HL-60 cells to undergo neutrophilic differentiation following ATRA exposure. p21 expression decreased significantly, suggesting Gfi-1 $^{-/-}$  + PPAR $\gamma$  $^{-/-}$  mutants were less likely to G0-arrest following ATRA exposure. The expression of other neutrophilic markers, such as CD38, also decreased in Gfi-1 $^{-/-}$  + PPAR $\gamma$  $^{-/-}$  cells. On the other hand, the expression of reactive oxygen metabolic markers, or other important transcription factors such as Oct4 did not change. For example, model analysis suggested that the C/EBP $\alpha$  dependent interaction of PU.1 with the *NCF1* gene, which encodes the p47Phox protein, was the most sensitive PU.1 connection; deletion of this connection removed the ability of the system to express p47Phox. p47Phox, also known as neutrophil cytosol factor 1, is one of four cytosolic subunits of the multi-protein NADPH oxidase complex found in neutrophils (41). This enzyme is responsible for reactive oxygen species (ROS) production, a key component of the anti-microbial function of neutrophils. While p47Phox expression required C/EBP $\alpha$  and PU.1, neither Gfi-1 nor PPAR $\gamma$  deletion increased expression. This suggested that p47Phox expression was saturated with respect to C/EBP $\alpha$  and PU.1, and simultaneously not sensitive to PPAR $\gamma$  abundance. Taken together, Gfi-1 $^{-/-}$  + PPAR $\gamma$  $^{-/-}$  cells were predicted to exhibit some aspects of the ATRA response, but not other critical features such as cell cycle arrest. Hock et al showed that Gfi-1 $^{-/-}$  mice lacked normal neutrophils, and were highly sensitive to bacterial infection (42). Thus, the model analysis was consistent with this study. However, other predictions concerning the behavior of the Gfi-1 $^{-/-}$  + PPAR $\gamma$  $^{-/-}$  mutants have yet to be verified experimentally.

Immunoprecipitation studies identified a limited number of ATRA-dependent and - independent Raf interaction partners. While we were unable to detect the association

353 of Raf with common kinases and GTPases such as PKC, PKA, p38, Rac and Rho, we  
354 did establish potential interactions between Raf and key partners such as Vav1, Src, Akt,  
355 CK2 and 14-3-3. All of these partners are known to be associated with Raf activation  
356 or function. Src is known to bind Raf through an SH2 domain, and this association has  
357 been shown to be dependent of the serine phosphorylation of Raf (43). Thus, an ATRA in-  
358 ductible Src/Raf association may be a result of ATRA-induced Raf phosphorylation at S259  
359 or S621. We also identified an interaction between Raf and the Ser/Thr kinases Akt and  
360 CK2. Akt can phosphorylate Raf at S259, as demonstrated by studies in a human breast  
361 cancer line (44). CK2 can also phosphorylate Raf, although the literature has traditionally  
362 focused on S338 and not S621 or S259(45). However, neither of these kinase interactions  
363 were ATRA-inducible, suggesting their association with Raf alone was not associated with  
364 ATRA-induced Raf phosphorylation. The adapter protein 14-3-3 was also constitutively  
365 associated with Raf. The interaction between Raf and 14-3-3 has been associated with  
366 both S621 and S259 phosphorylation and activity (46). Additionally, the association of  
367 Raf with 14-3-3 not only stabilized S621 phosphorylation, but also reversed the S621  
368 phosphorylation from inhibitory to activating (47). Finally, we found that Vav1/Raf associ-  
369 ation correlated with Raf activity, was ATRA-inducible and decreased after treatment with  
370 GW5074. The presence of Vav1 in Raf/Grb2 complexes has been shown to correlate with  
371 increased Raf activity in mast cells (48). Furthermore, studies on Vav1 knockout mice  
372 demonstrated that the loss of Vav1 resulted in deficiencies of ERK signaling for both T-  
373 cells as well as neutrophils (49, 50). Interestingly, while an integrin ligand-induced ROS  
374 response was blocked in Vav1 knockout neutrophils, TPA was able to bypass the Vav1  
375 requirement and stimulate both ERK phosphorylation and ROS induction (50). In this  
376 study, the TPA-induced ROS response was dependent upon Raf kinase activity, and was  
377 mitigated by the addition of GW5074. It is possible that Vav1 is downstream of various  
378 integrin receptors but upstream of Raf in terms of inducible ROS responses. Vav1 has

379 also been shown to associate with a Cbl-Slp76-CD38 complex in an ATRA-dependent  
380 manner; furthermore, transfection of HL-60 cells with Cbl mutants that fail to bind CD38,  
381 yet still bind Slp76 and Vav1, prevents ATRA-induced MAPK activation (15). The literature  
382 suggest a variety of possible receptor-signaling pathways, which involve Vav1, for MAPK  
383 activation; moreover, given the ATRA-inducible association Vav1 may play a direct role in  
384 Raf activation.

385 We hypothesized that Vav1 is a member of an ATRA-inducible complex which propels  
386 sustained MAPK activation, arrest and differentiation. Initially, ATRA-induced Vav1 ex-  
387 pression drives increased association between Vav1 and Raf. This increased interaction  
388 facilitates phosphorylation and activation of Raf by pre-bound Akt and/or CK2 at S621  
389 or perhaps S259. Constitutively bound 14-3-3 may also stabilize the S621 phosphory-  
390 lation, modulate the activity and/or up-regulate autophosphorylation. Activated Raf can  
391 then drive ERK activation, which in turn closes the positive feedback loop by activating  
392 Raf transcription factors e.g., Sp1 and/or STAT1 (51–54). We tested this working hy-  
393 pothesis using mathematical modeling. The model recapitulated both ATRA time-course  
394 data as well as the GW5074 inhibitor effects. This suggested the proposed Raf-Vav1  
395 architecture was at least consistent with the experimental studies. Further, analysis of  
396 the Raf-Vav1 model identified bistability in ppERK levels. Thus, two possible MAPK ac-  
397 tivation branches were possible for experimentally testable ATRA values. The analysis  
398 also suggested the ATRA-induced Raf-Vav1 architecture could be locked into a sustained  
399 signaling mode (high ppERK) even in the absence of a ATRA signal. This locked-in prop-  
400 erty could give rise to an ATRA-induction memory. We validated the treatment memory  
401 property predicted by the Raf-Vav1 circuit experimentally using ATRA-washout experi-  
402 ments. ERK phosphorylation levels remained high for more then 96 hr after ATRA was  
403 removed. Previous studies demonstrated that HL-60 cells possessed an inheritable mem-  
404 ory of ATRA stimulus (55). Although the active state was self-sustaining, the inactive state

405 demonstrated considerable robustness to perturbation. For example, we found that 50x  
406 overexpression of Raf was required to reliably lock MAPK into the activated state, while  
407 small perturbations had almost no effect on ppERK levels over the entire ensemble. CD38  
408 expression correlated with the ppERK, suggesting its involvement in the signaling com-  
409 plex. Our computational and experimental results showed that positive feedback, through  
410 ERK-dependent Raf expression, could sustain MAPK signaling through many division cy-  
411 cles. Such molecular mechanisms could underly aspects of cellular memory associated  
412 to consecutive ATRA treatments.

413 **Materials and Methods**

414 *Effective gene expression model equations.* The ATRA differentiation model was en-  
 415 coded as a system of differential algebraic equations (DAEs). We decomposed the ATRA-  
 416 induced differentiation program into three modules; a signal initiation module that sensed  
 417 and transformed the ATRA signal into activated cRaf-pS621 and the ATRA-RAR/RXR  
 418 (activated Trigger) signals; a signal integration module that controlled the expression of  
 419 upstream transcription factors given cRaf-pS621 and activated Trigger signals; and a phe-  
 420 notype module which encoded the expression of functional differentiation markers from  
 421 the ATRA-inducible transcription factors. The output of the signal initiation module was  
 422 the input to the gene expression model. For each gene  $j = 1, 2, \dots, \mathcal{G}$ , we modeled both  
 423 the mRNA ( $m_j$ ), protein ( $p_j$ ) and signaling species abundance:

$$\frac{dm_j}{dt} = r_{T,j} - (\mu + \theta_{m,j}) m_j + \lambda_j \quad (1)$$

$$\frac{dp_j}{dt} = r_{X,j} - (\mu + \theta_{p,j}) p_j \quad (2)$$

$$\mathbf{g}(p_1, \dots, p_{\mathcal{G}}, \kappa) = \mathbf{0} \quad (3)$$

424 where signaling species abundance was governed by the non-linear algebraic equations  
 425  $\mathbf{g}(p_1, \dots, p_{\mathcal{G}}, \kappa) = \mathbf{0}$ . The model parameter vector is denoted by  $\kappa$ . The terms  $r_{T,j}$  and  
 426  $r_{X,j}$  denote the specific rates of transcription, and translation while the terms  $\theta_{m,j}$  and  $\theta_{p,j}$   
 427 denote first-order degradation constants for mRNA and protein, respectively. The specific  
 428 transcription rate  $r_{T,j}$  was modeled as the product of a kinetic term  $\bar{r}_{T,j}$  and a control  
 429 term  $u_j$  which described how the abundance of transcription factors, or other regulators  
 430 influenced the expression of gene  $j$ . The kinetic transcription term  $\bar{r}_{T,j}$  was modeled as:

$$\bar{r}_{T,j} = V_T^{\max} \left( \frac{L_{T,o}}{L_{T,j}} \right) \left( \frac{G_j}{K_T + G_j} \right) \quad (4)$$

431 where the maximum gene expression rate  $V_T^{max}$  was defined as the product of a char-  
 432 acteristic transcription rate constant ( $k_T$ ) and the abundance of RNA polymerase ( $R_1$ ),  
 433  $V_T^{max} = k_T (R_1)$ . The  $(L_{T,o}/L_{T,j})$  term denotes the ratio of transcription read lengths;  $L_{T,o}$   
 434 represents a characteristic gene length, while  $L_{T,j}$  denotes the length of gene  $j$ . Thus, the  
 435 ratio  $(L_{T,o}/L_{T,j})$  is a gene specific correction to the characteristic transcription rate  $V_T^{max}$ .  
 436 Lastly, the  $\lambda_j$  term denotes the constitutive rate of expression of gene  $j$ .

437 The gene expression control term  $0 \leq u_j \leq 1$  depended upon the combination of fac-  
 438 tors which influenced the expression of gene  $j$ . If the expression of gene  $j$  was influenced  
 439 by  $1, \dots, m$  factors, we modeled this relationship as  $u_j = \mathcal{I}_j(f_{1j}(\cdot), \dots, f_{mj}(\cdot))$  where  
 440  $0 \leq f_{ij}(\cdot) \leq 1$  denotes a regulatory transfer function quantifying the influence of factor  $i$   
 441 on the expression of gene  $j$ , and  $\mathcal{I}_j(\cdot)$  denotes an integration rule which combines the  
 442 individual regulatory inputs for gene  $j$  into a single control term. In this study, the integra-  
 443 tion rule governing gene expression was the weighted fraction of promoter configurations  
 444 that resulted in gene expression (56):

$$u_j = \frac{W_{R_{1,j}} + \sum_n W_{nj} f_{nj}}{1 + W_{R_{1,j}} + \sum_d W_{dj} f_{dj}} \quad (5)$$

445 The numerator, the weighted sum (with weights  $W_{nj}$ ) of promoter configurations leading to  
 446 gene expression, was normalized by all possible promoter configurations. The likelihood  
 447 of each configuration was quantified by the transfer function  $f_{nj}$  (which we modeled using  
 448 Hill like functions), while the lead term in the numerator  $W_{R_{1,j}}$  denotes the weight of con-  
 449 stitutive expression for gene  $j$ . Given this formulation, the rate of constitutive expression  
 450 was then given by:

$$\lambda_j = \bar{r}_{T,j} \left( \frac{W_{R_{1,j}}}{1 + W_{R_{1,j}}} \right) \quad (6)$$

451 If a gene expression process had no modifying factors,  $u_j = 1$ . Lastly, the specific trans-

452 lation rate was modeled as:

$$r_{X,j} = V_X^{max} \left( \frac{L_{X,o}}{L_{X,j}} \right) \left( \frac{m_j}{K_X + m_j} \right) \quad (7)$$

453 where  $V_X^{max}$  denotes a characteristic maximum translation rate estimated from literature,  
454 and  $K_X$  denotes a translation saturation constant. The characteristic maximum translation  
455 rate was defined as the product of a characteristic translation rate constant ( $k_X$ ) and  
456 the Ribosome abundance ( $R_2$ ),  $V_X^{max} = k_X (R_2)$ . As was the case for transcription, we  
457 corrected the characteristic translation rate by the ratio of the length of a characteristic  
458 transcription normalized by the length of transcript  $j$ .

459 *Signaling model equations.* The signal initiation, and integration modules required the  
460 abundance of cRaf-pS621 and ATRA-RAR/RXR (activated Trigger) as inputs. However,  
461 our base model described only the abundance of inactive proteins e.g., cRaf or RXR/RAR  
462 but not the activated forms. To address this issue, we estimated pseudo steady state  
463 approximations for the abundance of cRaf-pS621 and activated Trigger. The abundance  
464 of activated trigger ( $x_{a,1}$ ) was estimated directly from the RXR/RAR abundance ( $x_{u,1}$ ):

$$x_{a,1} \sim x_{u,1} \left( \frac{\alpha \cdot \text{ATRA}}{1 + \alpha \cdot \text{ATRA}} \right) \quad (8)$$

465 where  $\alpha$  denotes a gain parameter;  $\alpha = 0.0$  if ATRA is less than a threshold, and  $\alpha = 0.1$   
466 if ATRA is greater than the differentiation threshold. The abundance of cRaf-pS621 was  
467 estimated by making the pseudo steady state approximation on the cRaf-pS621 balance.  
468 The abundance of an activated signaling species  $i$  was given by:

$$\frac{dx_i}{dt} = r_{+,i}(\mathbf{x}, \mathbf{k}) - (\mu + k_{d,i}) x_i \quad i = 1, \dots, \mathcal{M} \quad (9)$$

469 The quantity  $x_i$  denotes concentration of signaling species  $i$ , while  $\mathcal{R}$  and  $\mathcal{M}$  denote  
 470 the number of signaling reactions and signaling species in the model, respectively. The  
 471 term  $r_{+,i}(\mathbf{x}, \mathbf{k})$  denotes the rate of generation of activated species  $i$ , while  $\mu$  denotes  
 472 the specific growth rate, and  $k_{d,i}$  denotes the rate constant controlling the non-specific  
 473 degradation of  $x_i$ . We neglected deactivation reactions e.g., phosphatase activities. We  
 474 assumed that signaling processes were fast compared to gene expression; this allowed  
 475 us to approximate the signaling balance as:

$$x_i^* \simeq \frac{r_{+,i}(\mathbf{x}, \mathbf{k})}{(\mu + k_{d,i})} \quad i = 1, \dots, \mathcal{M} \quad (10)$$

476 The generation rate was written as the product of a kinetic term ( $\bar{r}_{+,i}$ ) and a control term  
 477 ( $v_i$ ). The control terms  $0 \leq v_j \leq 1$  depended upon the combination of factors which in-  
 478 fluenced rate process  $j$ . If rate  $j$  was influenced by  $1, \dots, m$  factors, we modeled this  
 479 relationship as  $v_j = \mathcal{I}_j(f_{1j}(\cdot), \dots, f_{mj}(\cdot))$  where  $0 \leq f_{ij}(\cdot) \leq 1$  denotes a regulatory  
 480 transfer function quantifying the influence of factor  $i$  on rate  $j$ . The function  $\mathcal{I}_j(\cdot)$  is an  
 481 integration rule which maps the output of regulatory transfer functions into a control vari-  
 482 able. In this study, we used  $\mathcal{I}_j \in \{\min, \max\}$  and hill transfer functions (57). If a process  
 483 had no modifying factors,  $v_j = 1$ . The kinetic rate of cRaf-pS621 generation  $\bar{r}_{+,cRaf}$  was  
 484 modeled as:

$$\bar{r}_{+,cRaf} = k_{+,cRaf} x_s \left( \frac{x_{cRaf}}{K_{+,cRaf} + x_{cRaf}} \right) \quad (11)$$

485 where  $x_s$  denotes the signalsome abundance, and  $K_{+,cRaf}$  denotes a saturation constant  
 486 governing cRaf-pS621 formation. The formation of cRaf-pS621 was regulated by only a  
 487 single factor, the abundance of MAPK inhibitor, thus  $v_{+,cRaf}$  took the form:

$$v_{+,cRaf} = \left( 1 - \frac{I}{K_D + I} \right) \quad (12)$$

488 where  $I$  denotes the abundance of the MAPK inhibitor, and  $K_D$  denotes the inhibitor  
489 affinity.

490 *Estimation of gene expression model parameters.* We estimated parameters appearing  
491 in the mRNA and protein balances, the abundance of polymerases and ribosomes, tran-  
492 scription and translation rates, the half-life of a typical mRNA and protein, and typical  
493 values for the copies per cell of RNA polymerase and ribosomes from literature (Table 2).  
494 The saturation constants  $K_X$  and  $K_T$  were adjusted so that gene expression and trans-  
495 lation resulted in gene products on a biologically realistic concentration scale. Lastly, we  
496 calculated the concentration for gene  $G_j$  by assuming, on average, that a cell had two  
497 copies of each gene at any given time. Thus, the bulk of our gene expression model pa-  
498 rameters were based directly upon literature values, and were not adjusted during model  
499 identification. However, the remaining parameters, e.g., the  $W_{ij}$  appearing in the gene  
500 expression control laws, or parameters appearing in the transfer functions  $f_{dij}$ , were esti-  
501 mated from the protein expression and signaling data sets discussed here.

502 Signaling and gene expression model parameters were estimated by minimizing the  
503 squared difference between simulations and experimental protein data set  $j$ . We mea-  
504 sured the squared difference in the scale, fold change and shape for protein  $j$ :

$$E_j(\mathbf{k}) = \left( \mathcal{M}_j(t_-) - \hat{y}_j(t_-, \mathbf{k}) \right)^2 + \sum_{i=1}^{\mathcal{T}_j} \left( \hat{\mathcal{M}}_{ij} - \hat{y}_{ij}(\mathbf{k}) \right)^2 + \sum_{i=1}^{\mathcal{T}_j} \left( \mathcal{M}'_{ij} - y'_{ij}(\mathbf{k}) \right)^2 \quad (13)$$

505 The first term in Eq. (13) quantified the initial *scale* error, directly before the addition  
506 of ATRA. In this case,  $\mathcal{M}_j(t_-)$  (the approximate concentration of protein  $j$  before the  
507 addition of ATRA) was estimated from literature. This term was required because the  
508 protein measurements were reported as the fold-change; thus, the data was normalized  
509 by a control value measured before the addition of ATRA. However, the model operated on  
510 a physical scale. The first term allowed the model to capture physically realistic changes

following ATRA addition. The second term quantified the difference in the *fold-change* of protein  $j$  as a function of time. The terms  $\hat{\mathcal{M}}_{ij}$  and  $\hat{y}_{ij}$  denote the scaled experimental observations and simulation outputs (fold-change; protein normalized by control value directly before ATRA addition) at time  $i$  from protein  $j$ , where  $T_j$  denoted the number of time points for data set  $j$ . Lastly, the third term of the objective function measured the difference in the *shape* of the measured and simulated protein levels. The scaled value  $0 \leq \mathcal{M}'_{ij} \leq 1$  was given by:

$$\hat{\mathcal{M}}_{ij} = \left( \mathcal{M}_{ij} - \min_i \mathcal{M}_{ij} \right) / \left( \max_i \mathcal{M}_{ij} - \min_i \mathcal{M}_{ij} \right) \quad (14)$$

where  $\mathcal{M}'_{ij} = 0$  and  $\mathcal{M}'_{ij} = 1$  describe the lowest (highest) intensity bands. A similar scaling was used for the simulation output. We minimized the total model residual  $\sum_j E_j$  using a heuristic direct-search optimization procedure, subject to box constraints on the parameter values, starting from a random initial parameter guess. Each downhill step was archived and used for ensemble calculations. The optimization procedure (a covariance matrix adaptation evolution strategy) has been reported previously (58).

*Estimation of an effective cell cycle arrest model.* We formulated an effective N-order polynomial model of the fraction of cells undergoing ATRA-induced cell cycle arrest at time  $t$ ,  $\hat{\mathcal{A}}(t)$ , as:

$$\hat{\mathcal{A}}(t) \simeq a_0 + \sum_{i=1}^{N-1} a_i \phi_i(\mathbf{p}(t), t) \quad (15)$$

where  $a_i$  were unknown parameters, and  $\phi_i(\mathbf{p}(t), t)$  denotes a basis function. The basis functions were dependent upon the system state; in this study, we assumed  $N = 4$  and basis functions of the form:

$$\phi_i(\mathbf{p}(t), t) = \left( \frac{t}{T} + \frac{p21}{E2F} \Big|_t \right)^{(i-1)} \quad (16)$$

530 The parameters  $a_0, \dots, a_3$  were estimated directly from cell-cycle measurements (biolog-  
531 ical replicates) using least-squares. The form of the basis function assumed p21 was  
532 directly proportional, and E2F inversely proportional to G0-arrest. However, this was only  
533 one form for the basis functions, many others are possible.

534 *Availability of the model code and parameters.* The signaling and gene expression model  
535 equations, and the parameter estimation procedure, were implemented in the Julia pro-  
536 gramming language. The model equations were solved using the ODE23s routine of the  
537 ODE package (59). The model code and parameter ensemble is available under an MIT  
538 software license and can be downloaded from <http://www.varnerlab.org>.

539 *Cell culture and treatment* Human myeloblastic leukemia cells (HL-60 cells) were grown  
540 in a humidified atmosphere of 5% CO<sub>2</sub> at 37°C and maintained in RPMI 1640 from Gibco  
541 (Carlsbad, CA) supplemented with 5% heat inactivated fetal bovine serum from Hyclone  
542 (Logan, UT) and 1× antibiotic/antimicotic (Gibco, Carlsbad, CA). Cells were cultured in  
543 constant exponential growth (60). Experimental cultures were initiated at  $0.1 \times 10^6$  cells/mL  
544 24 hr prior to ATRA treatment; if indicated, cells were also treated with GW5074 (2 $\mu$ M) 18  
545 hr before ATRA treatment. For the cell culture washout experiments, cells were treated  
546 with ATRA for 24 hr, washed 3x with prewarmed serum supplemented culture medium  
547 to remove ATRA, and reseeded in ATRA-free media as described. Western blot analysis  
548 was performed at incremental time points after removal of ATRA.

549 *Chemicals* All-Trans Retinoic Acid (ATRA) from Sigma-Aldrich (St. Louis, MO) was dis-  
550 solved in 100% ethanol with a stock concentration of 5mM, and used at a final concen-  
551 tration of 1 $\mu$ M (unless otherwise noted). The cRaf inhibitor GW5074 from Sigma-Aldrich  
552 (St. Louis, MO) was dissolved in DMSO with a stock concentration of 10mM, and used  
553 at a final concentration of 2 $\mu$ M. HL-60 cells were treated with 2 $\mu$ M GW5074 with or with-  
554 out ATRA (1 $\mu$ M) at 0 hr. This GW5074 dosage had a negligible effect on the cell cycle

555 distribution, compared to ATRA treatment alone.

556 *Immunoprecipitation and western blotting* For immunoprecipitation experiments, approx-  
557 imately  $1.2 \times 10^7$  cells were lysed as previously described. 300 $\mu$ g protein (in 300  $\mu$ L total  
558 volume) per sample was pre-cleared with Protein A/G beads. The beads were pelleted  
559 and supernatant was incubated with Raf antibody (3 $\mu$ L/sample) and beads overnight. All  
560 incubations included protease and phosphatase inhibitors in M-PER used for lysis with  
561 constant rotation at 4°C. Bead/antibody/protein slurries were then washed and subjected  
562 to standard SDS-PAGE analysis as previously described (15). All antibodies were pur-  
563 chased from Cell Signaling (Boston, MA) with the exception of  $\alpha$ -p621 Raf which was  
564 purchased from Biosource/Invitrogen (Carlsbad, CA), and  $\alpha$ -CK2 from BD Biosciences  
565 (San Jose, CA).

566 *Morphology assessment* Untreated and ATRA-treated HL-60 cells were collected after  
567 72 hr and cytocentrifuged for 3 min at 700 rpm onto glass slides. Slides were air-dried  
568 and stained with Wright's stain. Slide images were captured at 40X (Leica DM LB 100T  
569 microscope, Leica Microsystems).

570 **Competing interests**

571 The authors declare that they have no competing interests.

572 **Author's contributions**

573 J.V and A.Y directed the study. R.T, H.J, R.B and J.C conducted the cell culture measure-  
574 ments. J.V, R.B, W.D, K.R and A.S developed the reduced order HL-60 models and the  
575 parameter ensemble. W.D and J.V analyzed the model ensemble, and generated figures  
576 for the manuscript. The manuscript was prepared and edited for publication by W.D, R.B,  
577 A.Y and J.V.

578 **Acknowledgements**

579 We gratefully acknowledge the suggestions from the anonymous reviewers to improve  
580 this manuscript.

581 **Funding**

582 We acknowledge the financial support to J.V. by the National Science Foundation CA-  
583 REER (CBET-0846876) for the support of R.T. and H.J. In addition, we acknowledge  
584 support to A.Y. from the National Institutes of Health (CA 30555, CA152870) and a grant  
585 from New York State Stem Cell Science. Lastly, we acknowledge the financial support to  
586 J.V. and A.Y. from the National Cancer Institute (#U54 CA143876). The content is solely  
587 the responsibility of the authors and does not necessarily represent the official views of  
588 the National Cancer Institute or the National Institutes of Health.

589 **References**

- 590 1. Bushue N, Wan YJY (2010) Retinoid pathway and cancer therapeutics. *Adv Drug  
591 Deliv Rev* 62: 1285-98.
- 592 2. Tang XH, Gudas LJ (2011) Retinoids, retinoic acid receptors, and cancer. *Annu Rev  
593 Pathol* 6: 345-64.
- 594 3. Cheung FSG, Lovicu FJ, Reichardt JKV (2012) Current progress in using vitamin d  
595 and its analogs for cancer prevention and treatment. *Expert Rev Anticancer Ther*  
596 12: 811-37.
- 597 4. Nilsson B (1984) Probable in vivo induction of differentiation by retinoic acid of  
598 promyelocytes in acute promyelocytic leukaemia. *Br J Haematol* 57: 365-71.
- 599 5. Coombs CC, Tavakkoli M, Tallman MS (2015) Acute promyelocytic leukemia: where  
600 did we start, where are we now, and the future. *Blood Cancer J* 5: e304.
- 601 6. Warrell RP Jr (1993) Retinoid resistance in acute promyelocytic leukemia: new  
602 mechanisms, strategies, and implications. *Blood* 82: 1949-53.
- 603 7. Freemantle SJ, Spinella MJ, Dmitrovsky E (2003) Retinoids in cancer therapy and  
604 chemoprevention: promise meets resistance. *Oncogene* 22: 7305-15.
- 605 8. Harrison JS, Wang X, Studzinski GP (2016) The role of vdr and bim in potentiation  
606 of cytarabine-induced cell death in human aml blasts. *Oncotarget* 7: 36447-36460.
- 607 9. Breitman TR, Selonick SE, Collins SJ (1980) Induction of differentiation of the hu-  
608 man promyelocytic leukemia cell line (HL-60) by retinoic acid. *Proc Natl Acad Sci U  
609 S A* 77: 2936–2940.
- 610 10. Yen A, Roberson MS, Varvayanis S, Lee AT (1998) Retinoic acid induced  
611 mitogen-activated protein (MAP)/extracellular signal-regulated kinase (ERK) kinase-  
612 dependent MAP kinase activation needed to elicit HL-60 cell differentiation and  
613 growth arrest. *Cancer Res* 58: 3163–3172.
- 614 11. Hong HY, Varvayanis S, Yen A (2001) Retinoic acid causes MEK-dependent RAF

- 615 phosphorylation through RARalpha plus RXR activation in HL-60 cells. Differentiation 68: 55–66.
- 616
- 617 12. Mangelsdorf DJ, Ong ES, Dyck JA, Evans RM (1990) Nuclear receptor that identifies
- 618 a novel retinoic acid response pathway. Nature 345: 224–229.
- 619 13. Congleton J, MacDonald R, Yen A (2012) Src inhibitors, PP2 and dasatinib, increase
- 620 retinoic acid-induced association of Lyn and c-Raf (S259) and enhance MAPK-
- 621 dependent differentiation of myeloid leukemia cells. Leukemia 26: 1180-8.
- 622 14. Shen M, Bunaci R, Congleton J, Jensen H, Sayam L, et al. (2011) Interferon regu-
- 623 latory factor-1 binds c-Cbl, enhances mitogen activated protein kinase signaling and
- 624 promotes retinoic acid-induced differentiation of HL-60 human myelo-monoblastic
- 625 leukemia cells. Leuk Lymphoma 52: 2372-9.
- 626 15. Shen M, Yen A (2009) c-cbl tyrosine kinase-binding domain mutant g306e abolishes
- 627 the interaction of c-cbl with cd38 and fails to promote retinoic acid-induced cell dif-
- 628 ferentiation and g0 arrest. J Biol Chem 284: 25664-77.
- 629 16. Yen A, Varvayanis S, Smith J, Lamkin T (2006) Retinoic acid induces expression of
- 630 SLP-76: expression with c-FMS enhances ERK activation and retinoic acid-induced
- 631 differentiation/G0 arrest of HL-60 cells. Eur J Cell Biol 85: 117–132.
- 632 17. Marchisio M, Bertagnolo V, Colamussi ML, Capitani S, Neri LM (1998) Phos-
- 633 phatidylinositol 3-kinase in HL-60 nuclei is bound to the nuclear matrix and increases
- 634 during granulocytic differentiation. Biochem Biophys Res Commun 253: 346-51.
- 635 18. Congleton J, Jiang H, Malavasi F, Lin H, Yen A (2011) ATRA-induced HL-60 myeloid
- 636 leukemia cell differentiation depends on the CD38 cytosolic tail needed for mem-
- 637 brane localization, but CD38 enzymatic activity is unnecessary. Exp Cell Res 317:
- 638 910–919.
- 639 19. Wang J, Yen A (2004) A novel retinoic acid-responsive element regulates retinoic
- 640 acid induced BLR1 expression. Mol Cell Biol 24: 2423 - 2443.

- 641 20. Yen A (1990) HL-60 cells as a model of growth and differentiation: the significance  
642 of variant cells. *Hematology Review* 4: 5-46.
- 643 21. Yang T, Xiong Q, Enslen H, Davis R, Chow CW (2002) Phosphorylation of NFATc4  
644 by p38 mitogen-activated protein kinases. *Mol Cell Biol* 22: 3892–3904.
- 645 22. Wang J, Yen A (2008) A MAPK-positive Feedback Mechanism for BLR1 Signaling  
646 Propels Retinoic Acid-triggered Differentiation and Cell Cycle Arrest. *J Biol Chem*  
647 283: 4375–4386.
- 648 23. Geil WM, Yen A (2014) Nuclear raf-1 kinase regulates the cxcr5 promoter by asso-  
649 ciating with nfatc3 to drive retinoic acid-induced leukemic cell differentiation. *FEBS*  
650 *J* 281: 1170-80.
- 651 24. Tasseeff R, Nayak S, Song S, Yen A, Varner J (2011) Modeling and analysis of retinoic  
652 acid induced differentiation of uncommitted precursor cells. *Integr Biol* 3: 578 - 591.
- 653 25. Jensen HA, Styskal LE, Tasseeff R, Bunaciu RP, Congleton J, et al. (2013) The  
654 src-family kinase inhibitor pp2 rescues inducible differentiation events in emergent  
655 retinoic acid-resistant myeloblastic leukemia cells. *PLoS One* 8: e58621.
- 656 26. Jensen HA, Bunaciu RP, Ibabao CN, Myers R, Varner JD, et al. (2014) Retinoic acid  
657 therapy resistance progresses from unilineage to bilineage in hl-60 leukemic blasts.  
658 *PLoS One* 9: e98929.
- 659 27. Jensen HA, Bunaciu RP, Varner JD, Yen A (2015) Gw5074 and pp2 kinase inhibitors  
660 implicate nontraditional c-raf and lyn function as drivers of retinoic acid-induced mat-  
661 uration. *Cell Signal* 27: 1666-75.
- 662 28. Jensen HA, Yourish HB, Bunaciu RP, Varner JD, Yen A (2015) Induced myelomono-  
663 cytic differentiation in leukemia cells is accompanied by noncanonical transcription  
664 factor expression. *FEBS Open Bio* 5: 789-800.
- 665 29. Milo R, Jorgensen P, Moran U, Weber G, Springer M (2010) Bionumbers—the  
666 database of key numbers in molecular and cell biology. *Nucleic Acids Res* 38: D750-

- 667 3.
- 668 30. Katagiri K, Hattori S, Nakamura S, Yamamoto T, Yoshida T, et al. (1994) Activation  
669 of ras and formation of gap complex during tpa-induced monocytic differentiation of  
670 hl-60 cells. *Blood* 84: 1780–1789.
- 671 31. Miranda MB, Johnson DE (2007) Signal transduction pathways that contribute to  
672 myeloid differentiation. *Leukemia* 21: 1363–1377.
- 673 32. Hickstein DD, Back AL, Collins SJ (1989) Regulation of expression of the cd11b and  
674 cd18 subunits of the neutrophil adherence receptor during human myeloid differen-  
675 tiation. *J Biol Chem* 264: 21812–21817.
- 676 33. Hornstein I, Alcover A, Katzav S (2004) Vav proteins, masters of the world of cy-  
677 toskeleton organization. *Cell Signal* 16: 1-11.
- 678 34. Ferrell J (2002) Self-perpetuating states in signal transduction: positive feedback,  
679 double-negative feedback and bistability. *Curr Opin Cell Biol* 14: 140-8.
- 680 35. Laslo P, Spooner CJ, Warmflash A, Lancki DW, Lee HJ, et al. (2006) Multilineage  
681 transcriptional priming and determination of alternate hematopoietic cell fates. *Cell*  
682 126: 755-66.
- 683 36. Xiong W, Ferrell J (2003) A positive-feedback-based bistable 'memory module' that  
684 governs a cell fate decision. *Nature* 426: 460-5.
- 685 37. Bagci EZ, Vodovotz Y, Billiar TR, Ermentrout GB, Bahar I (2006) Bistability in apop-  
686 tosis: roles of bax, bcl-2, and mitochondrial permeability transition pores. *Biophys J*  
687 90: 1546-59.
- 688 38. Luan D, Zai M, Varner JD (2007) Computationally derived points of fragility of a  
689 human cascade are consistent with current therapeutic strategies. *PLoS Comput  
690 Biol* 3: e142.
- 691 39. Friedman AD (2007) Transcriptional control of granulocyte and monocyte develop-  
692 ment. *Oncogene* 26: 6816-28.

- 693 40. Dahl R, Walsh JC, Lancki D, Laslo P, Iyer SR, et al. (2003) Regulation of macrophage  
694 and neutrophil cell fates by the PU.1:C/EBPalpha ratio and granulocyte colony-  
695 stimulating factor. *Nat Immunol* 4: 1029-36.
- 696 41. El-Benna J, Dang PMC, Gougerot-Pocidalo MA, Marie JC, Braut-Boucher F (2009)  
697 p47phox, the phagocyte nadph oxidase/nox2 organizer: structure, phosphorylation  
698 and implication in diseases. *Exp Mol Med* 41: 217-25.
- 699 42. Hock H, Hamblen MJ, Rooke HM, Traver D, Bronson RT, et al. (2003) Intrinsic re-  
700 quirement for zinc finger transcription factor gfi-1 in neutrophil differentiation. *Immuni-*  
701 *tity* 18: 109-20.
- 702 43. Cleghon V, Morrison DK (1994) Raf-1 interacts with fyn and src in a non-  
703 phosphotyrosine-dependent manner. *J Biol Chem* 269: 17749–17755.
- 704 44. Zimmermann S, Moelling K (1999) Phosphorylation and regulation of raf by akt (pro-  
705 tein kinase b). *Science* 286: 1741–1744.
- 706 45. Ritt DA, Zhou M, Conrads TP, Veenstra TD, Copeland TD, et al. (2007) Ck2 is a  
707 component of the ksr1 scaffold complex that contributes to raf kinase activation.  
708 *Curr Biol* 17: 179–184.
- 709 46. Hekman M, Wiese S, Metz R, Albert S, Troppmair J, et al. (2004) Dynamic changes  
710 in c-raf phosphorylation and 14-3-3 protein binding in response to growth factor stim-  
711 ulation: differential roles of 14-3-3 protein binding sites. *J Biol Chem* 279: 14074–  
712 14086.
- 713 47. Dhillon AS, Yip YY, Grindlay GJ, Pakay JL, Dangers M, et al. (2009) The c-terminus  
714 of raf-1 acts as a 14-3-3-dependent activation switch. *Cell Signal* 21: 1645–1651.
- 715 48. Song JS, Gomez J, Stancato LF, Rivera J (1996) Association of a p95 vav-containing  
716 signaling complex with the fcepsilonlonri gamma chain in the rbl-2h3 mast cell line.  
717 evidence for a constitutive in vivo association of vav with grb2, raf-1, and erk2 in an  
718 active complex. *J Biol Chem* 271: 26962–26970.

- 719 49. Costello PS, Walters AE, Mee PJ, Turner M, Reynolds LF, et al. (1999) The rho-  
720 family gtp exchange factor vav is a critical transducer of t cell receptor signals to the  
721 calcium, erk, and nf-kappab pathways. *Proc Natl Acad Sci U S A* 96: 3035–3040.
- 722 50. Graham D, Robertson C, Bautista J, Mascarenhas F, Diacovo M, et al. (2007)  
723 Neutrophil-mediated oxidative burst and host defense are controlled by a Vav-  
724 PLCgamma2 signaling axis in mice. *J Clin Invest* 117: 3445–3452.
- 725 51. Kim HS, Lim IK (2009) Phosphorylated extracellular signal-regulated protein kinases  
726 1 and 2 phosphorylate sp1 on serine 59 and regulate cellular senescence via tran-  
727 scription of p21sdi1/cip1/waf1. *J Biol Chem* 284: 15475–15486.
- 728 52. Milanini-Mongiat J, Pouyss?gur J, Pag?o G (2002) Identification of two sp1 phos-  
729 phorylation sites for p42/p44 mitogen-activated protein kinases: their implication in  
730 vascular endothelial growth factor gene transcription. *J Biol Chem* 277: 20631–  
731 20639.
- 732 53. Zhang Y, Cho YY, Petersen BL, Zhu F, Dong Z (2004) Evidence of stat1 phosphory-  
733 lation modulated by mapks, mek1 and msk1. *Carcinogenesis* 25: 1165–1175.
- 734 54. Li Z, Theus MH, Wei L (2006) Role of erk 1/2 signaling in neuronal differentiation of  
735 cultured embryonic stem cells. *Dev Growth Differ* 48: 513–523.
- 736 55. Yen A, Reece SL, Albright KL (1984) Dependence of hl-60 myeloid cell differentiation  
737 on continuous and split retinoic acid exposures: precommitment memory associated  
738 with altered nuclear structure. *J Cell Physiol* 118: 277–286.
- 739 56. Moon TS, Lou C, Tamsir A, Stanton BC, Voigt CA (2012) Genetic programs con-  
740 structed from layered logic gates in single cells. *Nature* 491: 249-53.
- 741 57. Wayman JA, Sagar A, Varner JD (2015) Dynamic modeling of cell-free biochemical  
742 networks using effective kinetic models. *Processes* 3: 138.
- 743 58. Igel C, Hansen N, Roth S (2007) Covariance matrix adaptation for multi-objective  
744 optimization. *Evol Comput* 15: 1-28.

- 745 59. Bezanson J, Edelman A, Karpinski S, Shah VB (2014) Julia: A fresh approach to  
746 numerical computing. CoRR abs/1411.1607.
- 747 60. Brooks SC, Kazmer S, Levin AA, Yen A (1996) Myeloid differentiation and retinoblas-  
748 toma phosphorylation changes in HL-60 cells induced by retinoic acid receptor- and  
749 retinoid X receptor-selective retinoic acid analogs. Blood 87: 227–237.
- 750 61. Rishi AK, Gerald TM, Shao ZM, Li XS, Baumann RG, et al. (1996) Regulation of the  
751 human retinoic acid receptor alpha gene in the estrogen receptor negative human  
752 breast carcinoma cell lines skbr-3 and mda-mb-435. Cancer Res 56: 5246-52.
- 753 62. Mueller BU, Pabst T, Fos J, Petkovic V, Fey MF, et al. (2006) Atra resolves the dif-  
754 ferentiation block in t(15;17) acute myeloid leukemia by restoring pu.1 expression.  
755 Blood 107: 3330-8.
- 756 63. Luo XM, Ross AC (2006) Retinoic acid exerts dual regulatory actions on the ex-  
757 pression and nuclear localization of interferon regulatory factor-1. Exp Biol Med  
758 (Maywood) 231: 619-31.
- 759 64. Sylvester I, Schöler HR (1994) Regulation of the oct-4 gene by nuclear receptors.  
760 Nucleic Acids Res 22: 901-11.
- 761 65. Drach J, McQueen T, Engel H, Andreeff M, Robertson KA, et al. (1994) Retinoic  
762 acid-induced expression of cd38 antigen in myeloid cells is mediated through  
763 retinoic acid receptor-alpha. Cancer Res 54: 1746-52.
- 764 66. Liu M, Iavarone A, Freedman LP (1996) Transcriptional activation of the human  
765 p21(waf1/cip1) gene by retinoic acid receptor. correlation with retinoid induction of  
766 u937 cell differentiation. J Biol Chem 271: 31723-8.
- 767 67. Bunaciu RP, Yen A (2013) 6-formylindolo (3,2-b)carbazole (ficz) enhances retinoic  
768 acid (ra)-induced differentiation of hl-60 myeloblastic leukemia cells. Mol Cancer 12:  
769 39.
- 770 68. Balmer JE, Blomhoff R (2002) Gene expression regulation by retinoic acid. J Lipid

- 771 Res 43: 1773-808.
- 772 69. Rosen ED, Hsu CH, Wang X, Sakai S, Freeman MW, et al. (2002) C/ebpalpha in-  
773 duces adipogenesis through ppargamma: a unified pathway. Genes Dev 16: 22-6.
- 774 70. Varley CL, Bacon EJ, Holder JC, Southgate J (2009) Foxa1 and irf-1 intermediary  
775 transcriptional regulators of ppargamma-induced urothelial cytodifferentiation. Cell  
776 Death Differ 16: 103-14.
- 777 71. Bruemmer D, Yin F, Liu J, Berger JP, Sakai T, et al. (2003) Regulation of the growth  
778 arrest and dna damage-inducible gene 45 (gadd45) by peroxisome proliferator-  
779 activated receptor gamma in vascular smooth muscle cells. Circ Res 93: e38-47.
- 780 72. Delerive P, De Bosscher K, Besnard S, Vanden Berghe W, Peters JM, et al. (1999)  
781 Peroxisome proliferator-activated receptor alpha negatively regulates the vascular  
782 inflammatory gene response by negative cross-talk with transcription factors nf-  
783 kappaB and ap-1. J Biol Chem 274: 32048-54.
- 784 73. Altiok S, Xu M, Spiegelman BM (1997) Ppargamma induces cell cycle withdrawal:  
785 inhibition of e2f/dp dna-binding activity via down-regulation of pp2a. Genes Dev 11:  
786 1987-98.
- 787 74. Fei J, Cook C, Gillespie M, Yu B, Fullen K, et al. (2011) Atherogenic  $\omega$ -6 lipids mod-  
788 ulate ppar- egr-1 crosstalk in vascular cells. PPAR Res 2011: 753917.
- 789 75. Song EK, Lee YR, Kim YR, Yeom JH, Yoo CH, et al. (2012) Naadp mediates insulin-  
790 stimulated glucose uptake and insulin sensitization by ppar $\gamma$  in adipocytes. Cell Rep  
791 2: 1607-19.
- 792 76. Szanto A, Nagy L (2005) Retinoids potentiate peroxisome proliferator-activated re-  
793 ceptor gamma action in differentiation, gene expression, and lipid metabolic pro-  
794 cesses in developing myeloid cells. Mol Pharmacol 67: 1935-43.
- 795 77. Han S, Sidell N, Fisher PB, Roman J (2004) Up-regulation of p21 gene expres-  
796 sion by peroxisome proliferator-activated receptor gamma in human lung carcinoma

- 797           cells. Clin Cancer Res 10: 1911-9.
- 798       78. Von Knethen A, Brüne B (2002) Activation of peroxisome proliferator-activated re-  
799           ceptor gamma by nitric oxide in monocytes/macrophages down-regulates p47phox  
800           and attenuates the respiratory burst. J Immunol 169: 2619-26.
- 801       79. Dispirito JR, Fang B, Wang F, Lazar MA (2013) Pruning of the adipocyte peroxisome  
802           proliferator-activated receptor  $\gamma$  cistrome by hematopoietic master regulator pu.1.  
803           Mol Cell Biol 33: 3354-64.
- 804       80. Chen H, Ray-Gallet D, Zhang P, Hetherington CJ, Gonzalez DA, et al. (1995) Pu.1  
805           (spi-1) autoregulates its expression in myeloid cells. Oncogene 11: 1549-60.
- 806       81. Steidl U, Rosenbauer F, Verhaak RGW, Gu X, Ebralidze A, et al. (2006) Essential  
807           role of jun family transcription factors in pu.1 knockdown-induced leukemic stem  
808           cells. Nat Genet 38: 1269-77.
- 809       82. Pahl HL, Scheibe RJ, Zhang DE, Chen HM, Galson DL, et al. (1993) The proto-  
810           oncogene pu.1 regulates expression of the myeloid-specific cd11b promoter. J Biol  
811           Chem 268: 5014-20.
- 812       83. Yuki H, Ueno S, Tatetsu H, Niiro H, Iino T, et al. (2013) Pu.1 is a potent tumor  
813           suppressor in classical hodgkin lymphoma cells. Blood 121: 962-70.
- 814       84. Li SL, Schlegel W, Valente AJ, Clark RA (1999) Critical flanking sequences of pu.1  
815           binding sites in myeloid-specific promoters. J Biol Chem 274: 32453-60.
- 816       85. Timchenko N, Wilson DR, Taylor LR, Abdelsayed S, Wilde M, et al. (1995) Autoreg-  
817           ulation of the human c/ebp alpha gene by stimulation of upstream stimulatory factor  
818           binding. Mol Cell Biol 15: 1192-202.
- 819       86. Lidonnici MR, Audia A, Soliera AR, Prisco M, Ferrari-Amorotti G, et al. (2010) Ex-  
820           pression of the transcriptional repressor gfi-1 is regulated by c/ebpalpha and is  
821           involved in its proliferation and colony formation-inhibitory effects in p210bcr/abl-  
822           expressing cells. Cancer Res 70: 7949-59.

- 823 87. D'Alo' F, Johansen LM, Nelson EA, Radomska HS, Evans EK, et al. (2003) The  
824 amino terminal and e2f interaction domains are critical for c/ebp alpha-mediated  
825 induction of granulopoietic development of hematopoietic cells. *Blood* 102: 3163-  
826 71.
- 827 88. Pan Z, Hetherington CJ, Zhang DE (1999) Ccaat/enhancer-binding protein activates  
828 the cd14 promoter and mediates transforming growth factor beta signaling in mono-  
829 cyte development. *J Biol Chem* 274: 23242-8.
- 830 89. Harris TE, Albrecht JH, Nakanishi M, Darlington GJ (2001) Ccaat/enhancer-binding  
831 protein-alpha cooperates with p21 to inhibit cyclin-dependent kinase-2 activity and  
832 induces growth arrest independent of dna binding. *J Biol Chem* 276: 29200-9.
- 833 90. Bauvois B, Durant L, Laboureau J, Barthélémy E, Rouillard D, et al. (1999) Upreg-  
834 ulation of cd38 gene expression in leukemic b cells by interferon types i and ii. *J*  
835 *Interferon Cytokine Res* 19: 1059-66.
- 836 91. Passioura T, Dolnikov A, Shen S, Symonds G (2005) N-ras-induced growth suppres-  
837 sion of myeloid cells is mediated by irf-1. *Cancer Res* 65: 797-804.
- 838 92. Dahl R, Iyer SR, Owens KS, Cuylear DD, Simon MC (2007) The transcriptional  
839 repressor gfi-1 antagonizes pu.1 activity through protein-protein interaction. *J Biol*  
840 *Chem* 282: 6473-83.
- 841 93. Duan Z, Horwitz M (2003) Targets of the transcriptional repressor oncoprotein gfi-1.  
842 *Proc Natl Acad Sci U S A* 100: 5932-7.
- 843 94. Chen H, Zhang P, Radomska HS, Hetherington CJ, Zhang DE, et al. (1996) Octamer  
844 binding factors and their coactivator can activate the murine pu.1 (spi-1) promoter.  
845 *J Biol Chem* 271: 15743-52.
- 846 95. Behre G, Whitmarsh AJ, Coghlan MP, Hoang T, Carpenter CL, et al. (1999) c-jun  
847 is a jnk-independent coactivator of the pu.1 transcription factor. *J Biol Chem* 274:  
848 4939-46.

- 849 96. Kardassis D, Papakosta P, Pardali K, Moustakas A (1999) c-jun transactivates the  
850 promoter of the human p21(waf1/cip1) gene by acting as a superactivator of the  
851 ubiquitous transcription factor sp1. *J Biol Chem* 274: 29572-81.
- 852 97. Johnson DG, Ohtani K, Nevins JR (1994) Autoregulatory control of e2f1 expression  
853 in response to positive and negative regulators of cell cycle progression. *Genes Dev*  
854 8: 1514-25.
- 855 98. Fu M, Zhang J, Lin Y, Zhu X, Ehrengruber MU, et al. (2002) Early growth response  
856 factor-1 is a critical transcriptional mediator of peroxisome proliferator-activated  
857 receptor-gamma 1 gene expression in human aortic smooth muscle cells. *J Biol  
858 Chem* 277: 26808-14.
- 859 99. Mak KS, Funnell APW, Pearson RCM, Crossley M (2011) Pu.1 and haematopoietic  
860 cell fate: Dosage matters. *Int J Cell Biol* 2011: 808524.
- 861 100. Chen F, Wang Q, Wang X, Studzinski GP (2004) Up-regulation of egr1 by 1,25-  
862 dihydroxyvitamin d3 contributes to increased expression of p35 activator of cyclin-  
863 dependent kinase 5 and consequent onset of the terminal phase of hl60 cell differ-  
864 entiation. *Cancer Res* 64: 5425-33.
- 865 101. Suh J, Jeon YJ, Kim HM, Kang JS, Kaminski NE, et al. (2002) Aryl hydrocarbon  
866 receptor-dependent inhibition of ap-1 activity by 2,3,7,8-tetrachlorodibenzo-p-dioxin  
867 in activated b cells. *Toxicol Appl Pharmacol* 181: 116-23.
- 868 102. Shen M, Bunaciu RP, Congleton J, Jensen HA, Sayam LG, et al. (2011) Inter-  
869 feron regulatory factor-1 binds c-cbl, enhances mitogen activated protein kinase  
870 signaling and promotes retinoic acid-induced differentiation of hl-60 human myelo-  
871 monoblastic leukemia cells. *Leuk Lymphoma* 52: 2372-9.
- 872 103. Bunaciu RP, Yen A (2011) Activation of the aryl hydrocarbon receptor ahr promotes  
873 retinoic acid-induced differentiation of myeloblastic leukemia cells by restricting ex-  
874 pression of the stem cell transcription factor oct4. *Cancer Res* 71: 2371-80.

- 875 104. Jackson DA, Pombo A, Iborra F (2000) The balance sheet for transcription: an anal-  
876 ysis of nuclear rna metabolism in mammalian cells. *FASEB J* 14: 242-54.
- 877 105. Zhao ZW, Roy R, Gebhardt JCM, Suter DM, Chapman AR, et al. (2014) Spatial orga-  
878 nization of rna polymerase ii inside a mammalian cell nucleus revealed by reflected  
879 light-sheet superresolution microscopy. *Proc Natl Acad Sci U S A* 111: 681-6.
- 880 106. Freitas R, Merkle R (2004) Kinematic Self-Replicating Machines. Oxford University  
881 Press.
- 882 107. Yang E, van Nimwegen E, Zavolan M, Rajewsky N, Schroeder M, et al. (2003) De-  
883 cay rates of human mrnas: correlation with functional characteristics and sequence  
884 attributes. *Genome Res* 13: 1863-72.
- 885 108. Doherty MK, Hammond DE, Clague MJ, Gaskell SJ, Beynon RJ (2009) Turnover  
886 of the human proteome: determination of protein intracellular stability by dynamic  
887 silac. *J Proteome Res* 8: 104-12.
- 888 109. Sehgal PB, Derman E, Molloy GR, Tamm I, Darnell JE (1976) 5,6-dichloro-1-beta-  
889 d-ribofuranosylbenzimidazole inhibits initiation of nuclear heterogeneous rna chains  
890 in hela cells. *Science* 194: 431-3.
- 891 110. Darzacq X, Shav-Tal Y, de Turris V, Brody Y, Shenoy SM, et al. (2007) In vivo dy-  
892 namics of rna polymerase ii transcription. *Nat Struct Mol Biol* 14: 796-806.
- 893 111. Kos M, Tollervey D (2010) Yeast pre-rrna processing and modification occur cotran-  
894 scriptionally. *Mol Cell* 37: 809-20.
- 895 112. Darnell JE Jr (2013) Reflections on the history of pre-mrna processing and highlights  
896 of current knowledge: a unified picture. *RNA* 19: 443-60.
- 897 113. Boström K, Wettsten M, Borén J, Bondjers G, Wiklund O, et al. (1986) Pulse-chase  
898 studies of the synthesis and intracellular transport of apolipoprotein b-100 in hep g2  
899 cells. *J Biol Chem* 261: 13800-6.
- 900 114. Meyers R, editor (2004) Encyclopedia of Molecular Cell Biology and Molecular

- 901 Medicine, Volume 1, 2nd Edition. ISBN: 978-3-527-30543-8. Wiley-Blackwell.
- 902 115. Rosenbluth MJ, Lam WA, Fletcher DA (2006) Force microscopy of nonadherent  
903 cells: a comparison of leukemia cell deformability. *Biophys J* 90: 2994-3003.
- 904 116. O'Leary NA, Wright MW, Brister JR, Ciufo S, Haddad D, et al. (2016) Reference  
905 sequence (refseq) database at ncbi: current status, taxonomic expansion, and func-  
906 tional annotation. *Nucleic Acids Res* 44: D733-45.
- 907 117. Wallace AS, Supnick HT, Bunaciu RP, Yen A (2016) Rrd-251 enhances all-trans  
908 retinoic acid (ra)-induced differentiation of hl-60 myeloblastic leukemia cells. *Oncot-  
909 target* 7: 46401.
- 910 118. Congleton J, MacDonald R, Yen A (2012) Src inhibitors, pp2 and dasatinib, in-  
911 crease retinoic acid-induced association of lyn and c-raf (s259) and enhance mapk-  
912 dependent differentiation of myeloid leukemia cells. *Leukemia* 26: 1180–1188.
- 913 119. Congleton J, Shen M, MacDonald R, Malavasi F, Yen A (2014) Phosphorylation of  
914 c-cbl and p85 pi3k driven by all-trans retinoic acid and cd38 depends on lyn kinase  
915 activity. *Cellular signalling* 26: 1589–1597.
- 916 120. Bunaciu RP, Jensen HA, MacDonald RJ, LaTocha DH, Varner JD, et al. (2015)  
917 6-formylindolo(3,2-b)carbazole (ficz) modulates the signalsome responsible for  
918 ra-induced differentiation of hl-60 myeloblastic leukemia cells. *PLoS One* 10:  
919 e0135668.
- 920 121. Shen M, Yen A (2008) c-cbl interacts with cd38 and promotes retinoic acid–induced  
921 differentiation and g0 arrest of human myeloblastic leukemia cells. *Cancer research*  
922 68: 8761–8769.

**Table 1:** Myelomonocytic transcription factor connectivity used in the signal integration and phenotype modules.

Effector	Effect	Target	Source
RAR $\alpha$	+	RAR $\alpha$	(61)
	+	PU.1	(62)
	+	C/EBP $\alpha$	(39)
	+	IRF-1	(63)
	-	Oct4	(64)
	+	CD38	(65)
	+	p21	(66)
	+	AhR	(67)
	+	Egr-1	(68)
PPAR $\gamma$	+	C/EBP $\alpha$	(69)
	+	IRF-1	(70)
	+	Oct1	(71)
	-	AP-1	(72)
	-	E2F	(73)
	-	Egr-1	(74)
	+	CD38	(75)
	+	CD14	(76)
	+	p21	(77)
	-	p47Phox	(78)
PU.1	-	PPAR $\gamma$	(79)
	+	PU.1	(80)
	+	AP-1	(81)
	+	Egr-1	(35)
	+	CD11b	(82)
	+	p21	(83)
	+	p47Phox	(84)
C/EBP $\alpha$	+	PPAR $\gamma$	(69)
	+	PU.1	(40)
	+	C/EBP $\alpha$	(85)
	+	Gfi-1	(86)
	-	E2F	(87)
	+	CD14	(88)

924

	+	p21	(89)
IRF-1	+	CD38	(90)
	+	p21	(91)
	-	PU.1	(92)
	-	C/EBP $\alpha$	(93)
	-	E2F	(93)
	-	Egr-1	(35)
	-	p21	(93)
Oct1	+	PU.1	(94)
AP-1	-	PPAR $\gamma$	(72)
	+	PU.1	(95)
	+	p21	(96)
E2F	+	E2F	(97)
Egr-1	+	PPAR $\gamma$	(98)
	-	Gfi-1	(99)
	+	CD14	(100)
AhR	+	AP-1	(101)
	+	IRF-1	(102)
	-	Oct4	(103)
	-	PU.1	

**Table 2:** Characteristic model parameters estimated from literature.

Symbol	Description	Value	Units	Source
$R_1$	RNA polymerase abundance	85,000	copies/cell	(104, 105)
$R_2$	Ribosome abundance	$1 \times 10^6$	copies/cell	(106)
$G_i$	Characteristic gene abundance	2	copies/cell	this study
$K_X$	Saturation constant transcription	600	copies/cell	this study
$K_T$	Saturation constant translation	95,000	copies/cell	this study
$t_{1/2,m}$	characteristic mRNA half-life (transcription factor)	2-4	hr	(107)
$t_{1/2,p}$	characteristic protein half-life	10	hr	(108)
$\theta_{m,j}$	characteristic mRNA degradation constant	0.34	$hr^{-1}$	derived
$\theta_{p,j}$	characteristic protein degradation constant	0.07	$hr^{-1}$	derived
927	$t_d$	HL-60 doubling time	19.5	hr
	$\mu$	growth rate	0.035	$hr^{-1}$
	$k_d$	death rate	$0.10\mu$	$hr^{-1}$
	$e_T$	elongation rate RNA polymerase	50-100	nt/s
	$e_X$	elongation rate Ribosome	5	aa/s
	$L_{T,o}$	characteristic gene length	15,000	nt
	$L_{X,o}$	characteristic transcript length	5,000	nt
	$k_T$	characteristic transcription rate	1.44	$hr^{-1}$
	$k_X$	characteristic translation rate	3.60	$hr^{-1}$
	$D$	Diameter of an HL-60 cell	12.4	$\mu m^3$
	$f_C$	cytoplasmic fraction	0.51	dimensionless

928 **Table 3:** Sequence lengths from NCBI RefSeq database was used in the signal integration and phenotype  
 929 modules (116). The RNA sequence length used represents the total distance of transcription, and assume  
 to be equal to the gene length.

Gene Name	Gene (bp)	RNA (bp)	Protein (AA)	Gene ID	Protein ID
AP-1	10323	10323	331	Gene ID: 3725	NP_002219
AhR	47530	47530	848	Gene ID: 196	NP_001621
CD11b	72925	72925	1153	Gene ID: 3684	NP_001139280
CD14	8974	8974	375	Gene ID: 929	NP_001035110
CD38	174978	74978	300	Gene ID: 952	NP_001766
C/EBP $\alpha$	2630	2630	393	Gene ID: 1050	NP_001274353.1
E2F	17919	17919	437	Gene ID: 1869	NP_005216
930 Egr-1	10824	10824	543	Gene ID: 1958	NP_001955
Gfi-1	13833	13833	422	Gene ID: 2672	NP_005254
IRF-1	16165	16165	325	Gene ID: 3659	NP_002189
Oct1	206516	206516	741.33	Gene ID: 5451	NP_002688.3, NP_001185712.1, NP_001185715.1
Oct4	6356	6356	206.33	Gene ID: 5460	NP_001167002, NP_001167015, NP_001167016
P21	15651	15651	198	NG_009364.1	NP_001621
P47	3074	3074	390	GenBank: AF003533.1	NP_000256
PPAR $\gamma$	153507	153507	250	Gene ID: 5468	NP_001317544
PU.1	40782	40782	270.5	Gene ID: 6688	NP_001074016, NP_003111

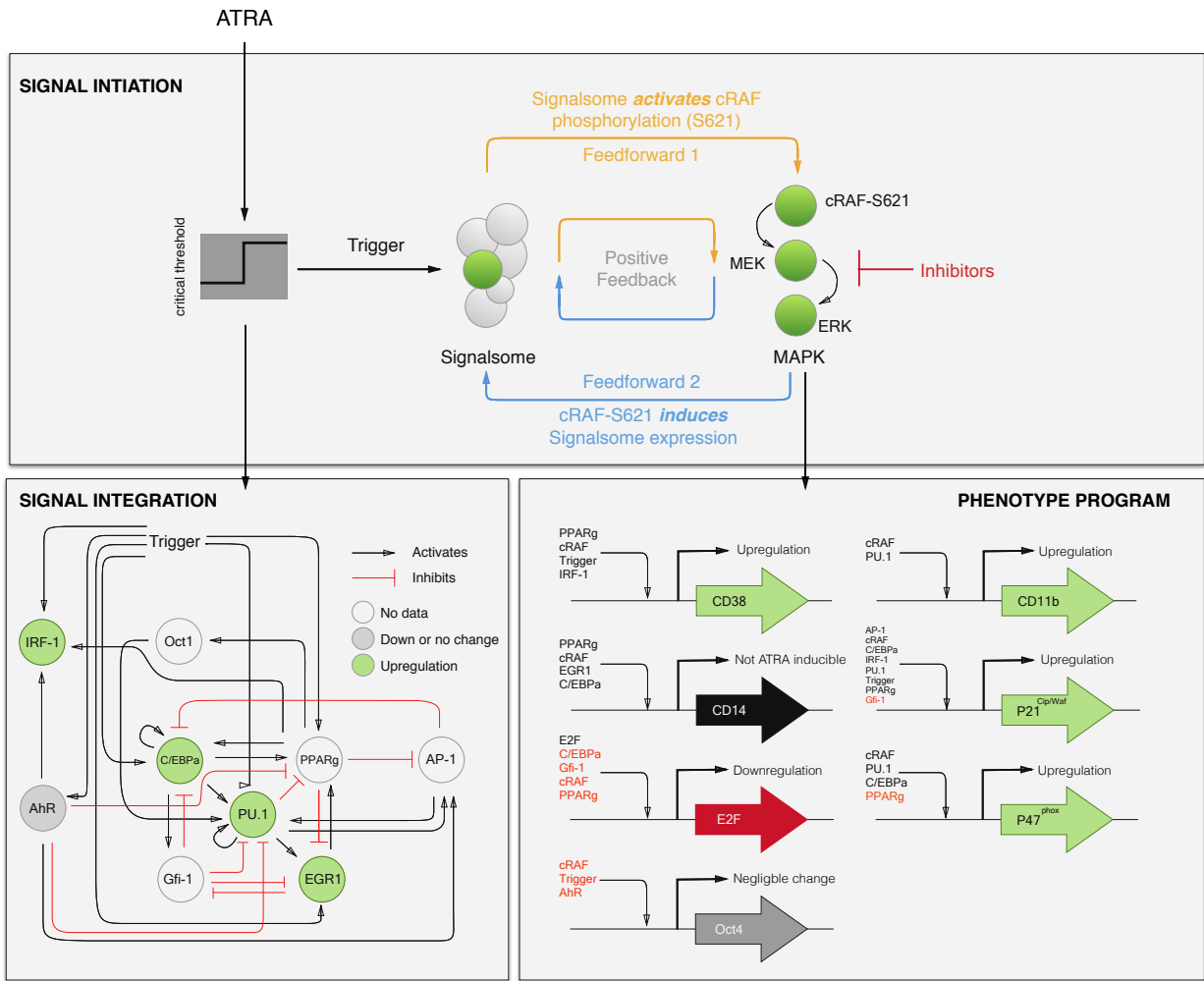


**Fig. 1:** Schematic of the effective ATRA differentiation circuit. Above a critical threshold, ATRA activates an upstream Trigger, which induces signalsome complex formation. Signalsome activates the mitogen-activated protein kinase (MAPK) cascade which in turn drives the differentiation program and signalsome formation. Both Trigger and activated cRaf-pS621 drive a phenotype gene expression program responsible for differentiation. Trigger activates the expression of a series of transcription factors which in combination with cRaf-pS621 result in phenotypic change.

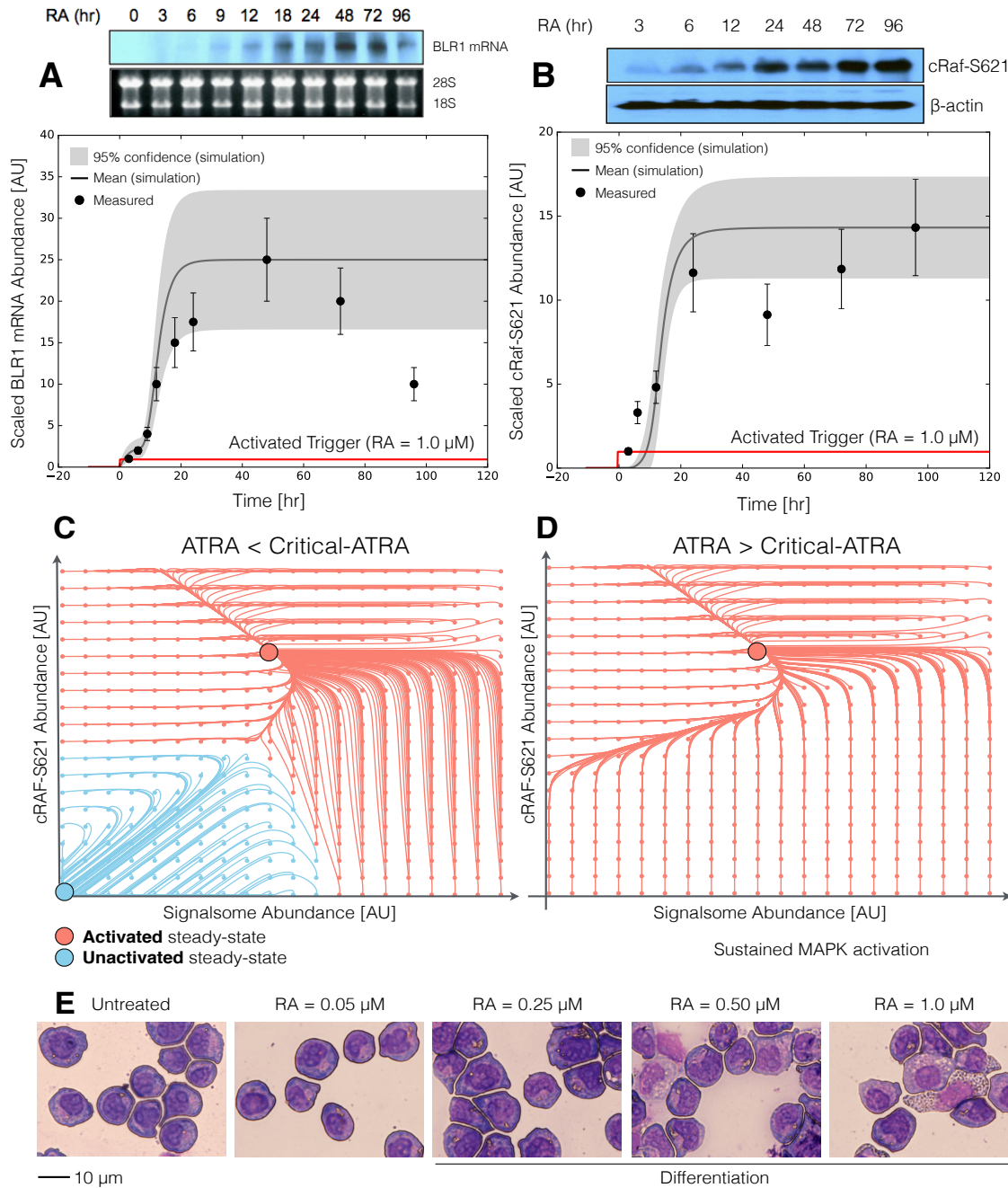


**Fig. 2:** Model analysis for ATRA-induced HL-60 differentiation. A: BLR1 mRNA versus time following exposure to 1  $\mu$ M ATRA at t = 0 hr. B: cRaf-pS621 versus time following exposure to 1  $\mu$ M ATRA at t = 0 hr. Points denote experimental measurements, solid lines denote the mean model performance. Shaded regions denote the 99% confidence interval calculated over the parameter ensemble. C: Signalsome and cRaf-pS621 nullclines for ATRA below the critical threshold. The model had two stable steady states and a single unstable state in this regime. D: Signalsome and cRaf-pS621 nullclines for ATRA above the critical threshold. In this regime the model had only a single stable steady state. E: Morphology of HL-60 as a function of ATRA concentration (t = 72 hr).

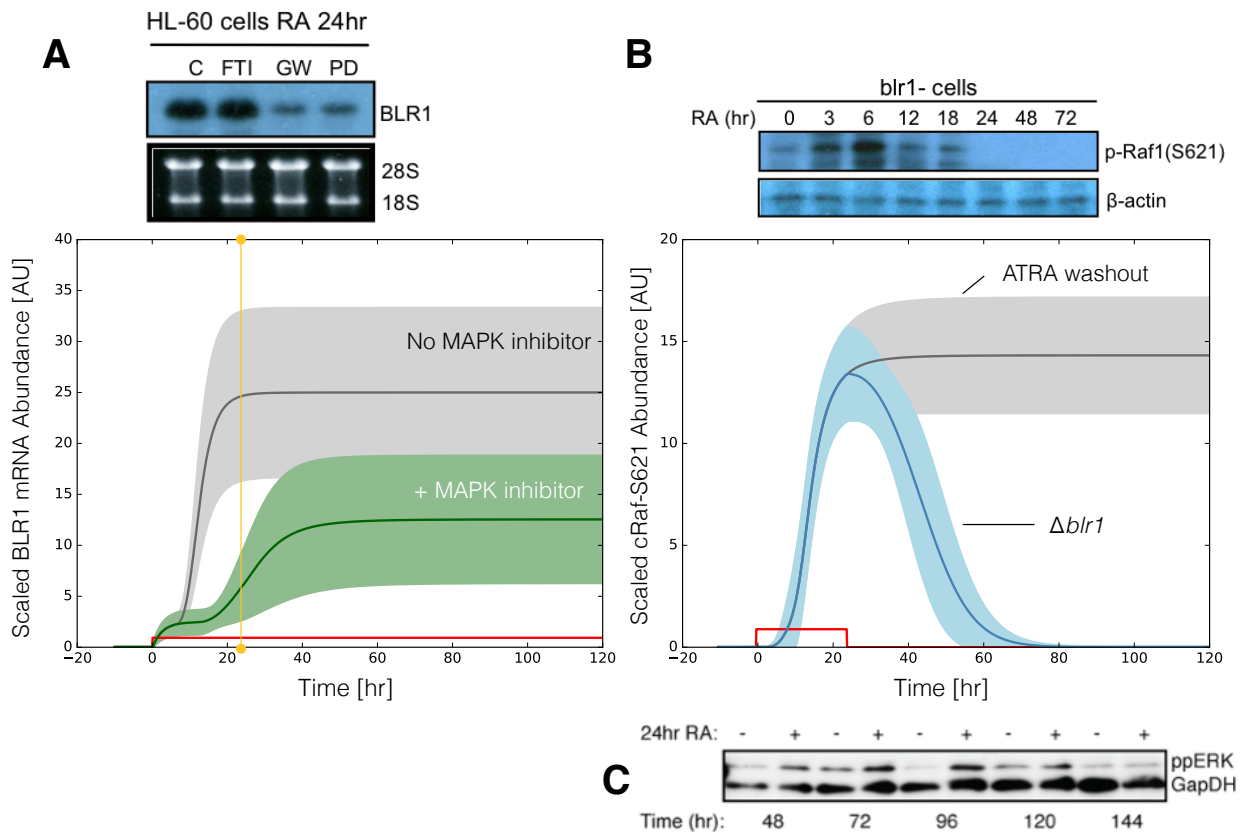


**Fig. 3:** Model simulation following exposure to  $1\mu\text{M}$  ATRA. A: BLR1 mRNA versus time with and without MAPK inhibitor. B: cRaf-pS621 versus time following pulsed exposure to  $1\mu\text{M}$  ATRA with and without BLR1. Solid lines denote the mean model performance, while shaded regions denote the 99% confidence interval calculated over the parameter ensemble. C: Western blot analysis of phosphorylated ERK1/2 in ATRA washout experiments. Experimental data in panels A and B were reproduced from Wang and Yen (22), data in panel C is reported in this study.

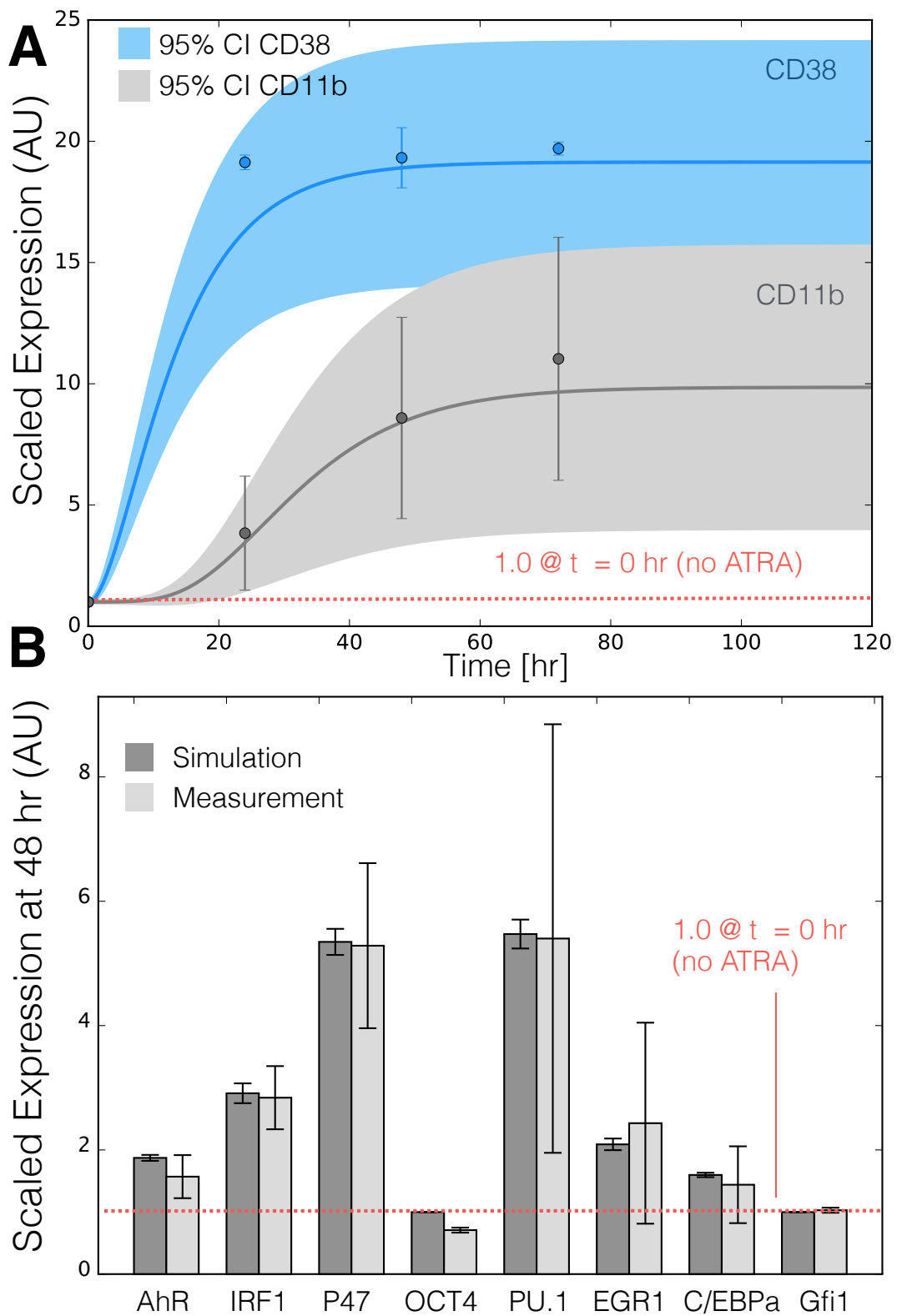


**Fig. 4:** Model simulation of the HL-60 gene expression program following exposure to  $1\mu\text{M}$  ATRA at  $t = 0$  hr. A: CD38 and CD11b expression versus time following ATRA exposure at time  $t = 0$  hr. B: Gene expression at  $t = 48$  hr following ATRA exposure. Experimental data in panels A and B were reproduced from Jensen et al. (28).

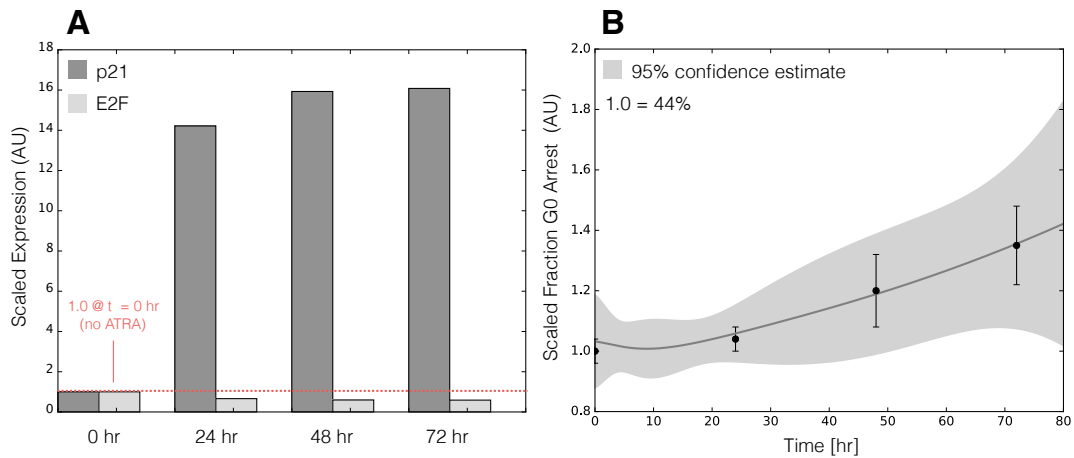


**Fig. 5:** Model simulation of HL-60 cell-cycle arrest following exposure to  $1\mu\text{M}$  ATRA at  $t = 0$  hr. A: Predicted p21 and E2F expression levels for the best parameter set following ATRA exposure at time  $t = 0$  hr. B: Estimated fraction of HL-60 cells in G0 arrest following ATRA exposure at time  $t = 0$  hr. The gray region denotes the 95% confidence estimate of the polynomial model. Experimental data in panel B was reproduced from Jensen et al. (28).

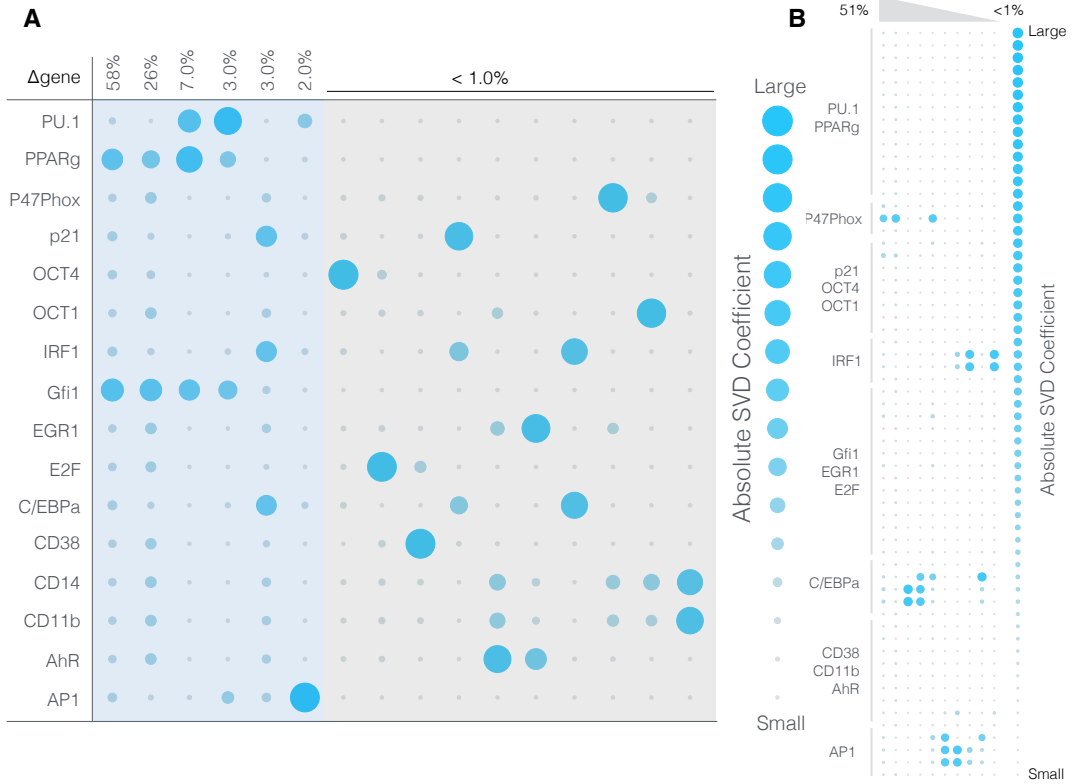


**Fig. 6:** Robustness of the HL-60 differentiation program following exposure to  $1\mu\text{M}$  ATRA at  $t = 0$  hr. A: Singular value decomposition of the system response ( $l^2$ -norm between the perturbed and nominal state) following pairwise gene knockout simulations using the best fit parameter set. The percentage at the top of each column describes the fraction of the variance in the system state captured by the node combinations in the rows. B: Singular value decomposition of the system response ( $l^2$ -norm between the perturbed and nominal state) following the pairwise removal of connections.

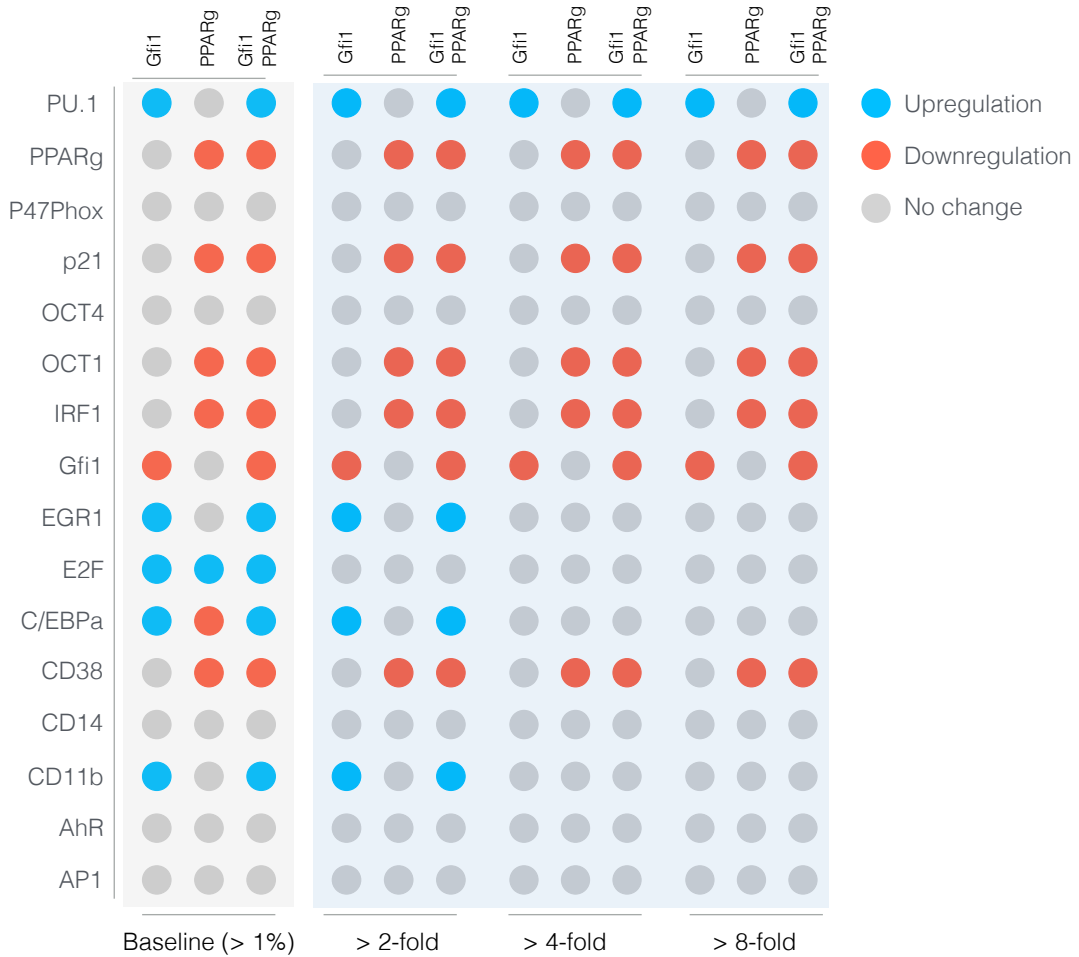


**Fig. 7:** Robustness of the HL-60 differentiation program following exposure to  $1\mu\text{M}$  ATRA at  $t = 0$  hr. Protein fold change at  $t = 48$  hr (rows) in single and double knock-out mutants (columns) relative to wild-type HL-60 cells. The responses were grouped into  $>2,4$  and  $8$  fold changes. The best fit parameter set was used to calculate the protein fold change.

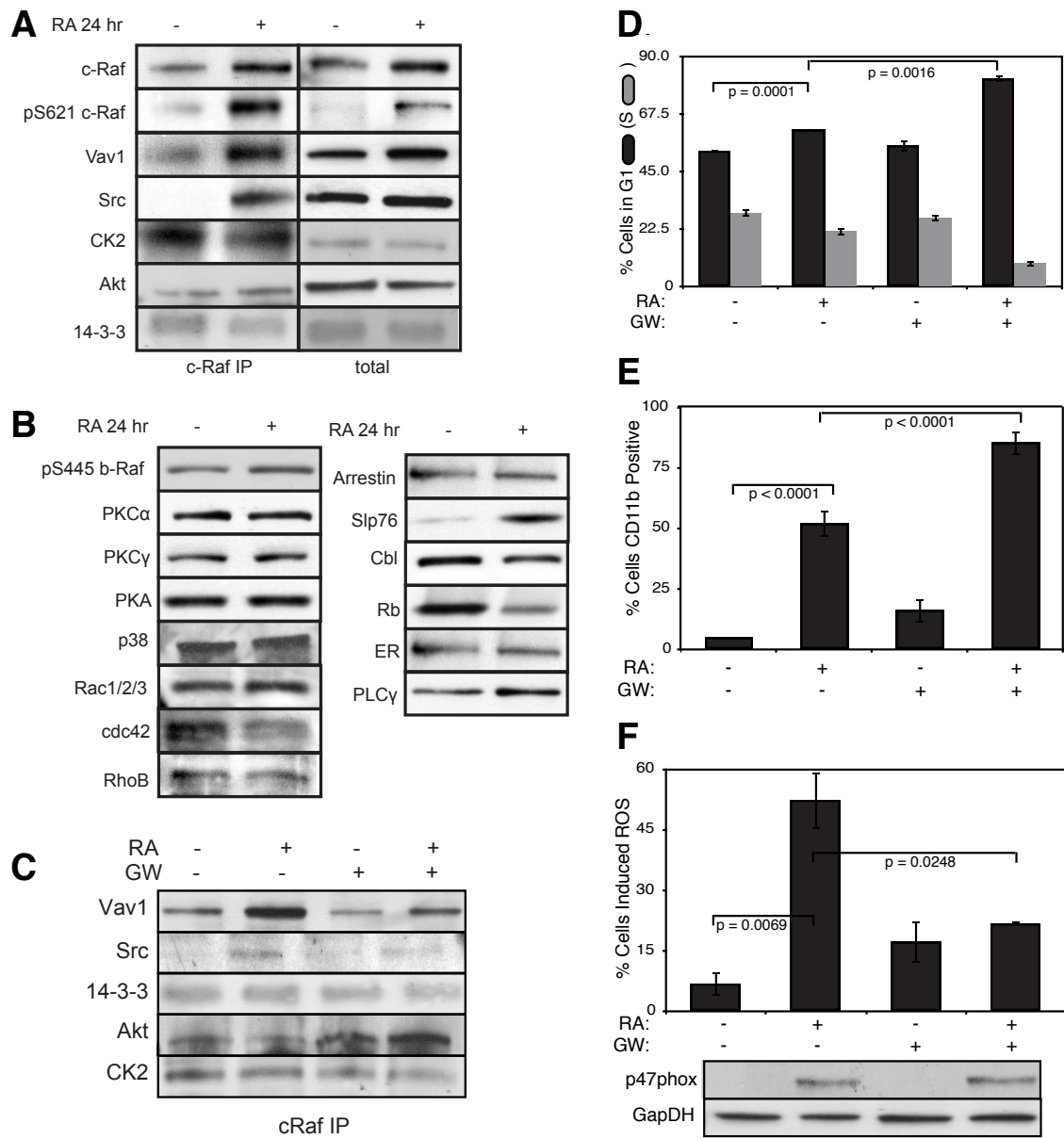


**Fig. 8:** Investigation of a panel of possible Raf interaction partners in the presence and absence of ATRA. A: Species identified to precipitate out with Raf: first column shows Western blot analysis on total Raf immunoprecipitation with and without 24 hr ATRA treatment and the second on total lysate. B: The expression of species considered that did not precipitate out with Raf at levels detectable by Western blot analysis on total lysate. C: Effect of the Raf inhibitor GW5074 on Raf interactions as determined by Western blot analysis of total Raf immunoprecipitation. The Authors note the signal associated with Src was found to be weak. D: Cell Cycle distribution as determined by flow cytometry indicated arrest induced by ATRA, which was increased by the addition of GW5074. E: Expression of the cell surface marker CD11b as determined by flow cytometry indicated increased expression induced by ATRA, which was enhanced by the addition of GW5074. F: Inducible reactive oxygen species (ROS) as determined by DCF flow cytometry. The functional differentiation response of ATRA treated cells was mitigated by GW5074.

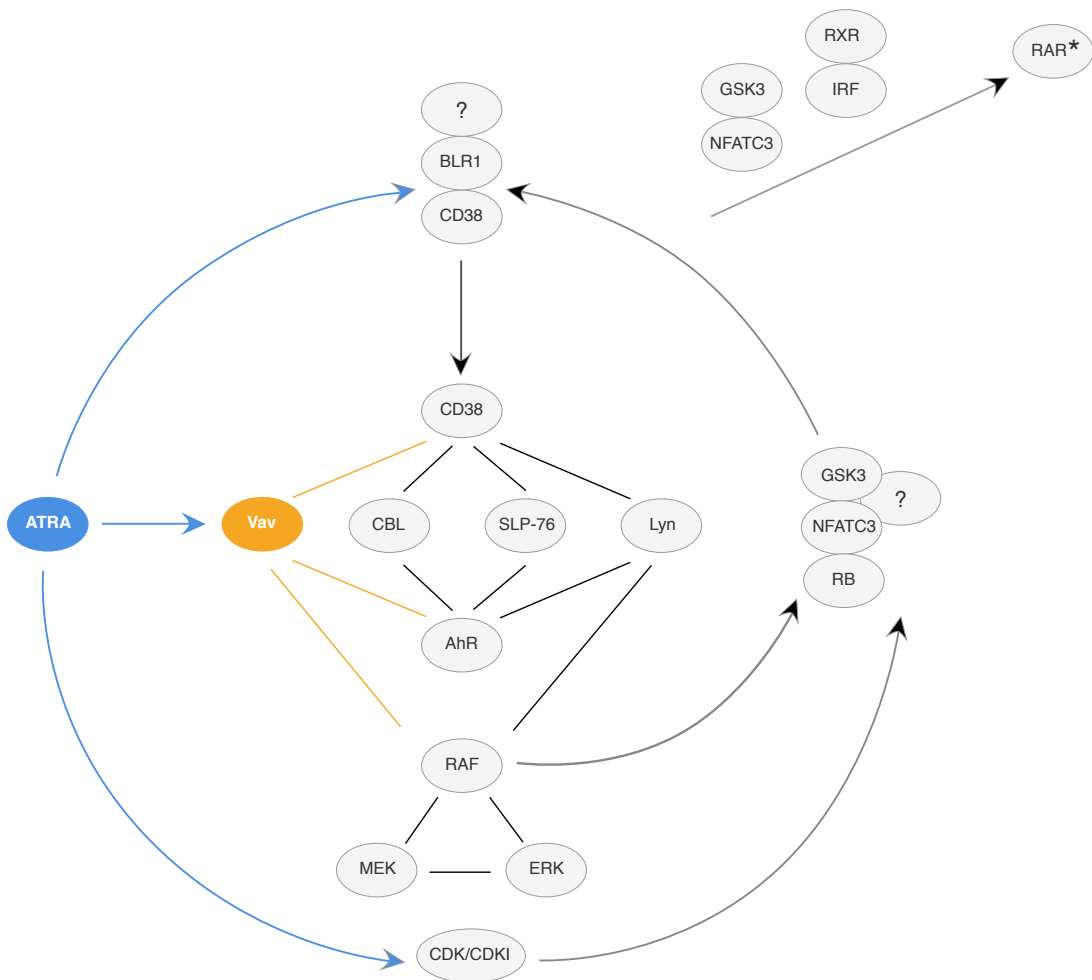


**Fig. 9:** Schematic of the hypothetical principal pathways in the ATRA-induced signaling that results in cell differentiation in the HL-60 myeloid leukemia model (15, 117–121). It is based on modules and feedback loops. There are three main arms (shown top to bottom): 1. Direct ATRA targeting of RAREs in genes such as CD38 or BLR1; 2. Formation of a signalsome that has a regulatory module that includes Vav (a GEF), CBL and SLP-76 (adaptors), and Lyn (a SFK) that regulates a Raf/Mek/Erk axis that incorporates Erk to Raf feedback, where the regulators are modulated by AhR and CD38 receptors; and 3. Direct ATRA targeted up regulation of CDKI to control RB hypophosphorylation. The Raf/Mek/Erk axis is embedded in the signalsome and subject to modulation by the regulators. The output of the signalsome is discharge of the Raf from the cytosol to the nucleus where it binds (hyper)phospho-RB and other targets, including NFATc3, which enables activation of the RA bound RAR/RXR poised on the BLR1 promoter, and also GSK3, phosphorylation of which relieves its inhibitory effect on RAR $\alpha$ . CDKI directed hypophosphorylation of RB releases Raf sequestered by RB to go to NFATc3, GSK3, and other targets. A significant consequence of the nuclear RAF is ergo ultimately to hyperactivate transcriptional activation by RAR $\alpha$  to drive differentiation. It might be noted that this general proposed model provides a mechanistic rationalization for why cell cycle arrest is historically oft times perceived as a feature predisposing phenotypic maturation.